Mariana Filipa Mestre Pina Amaro
Licenciatura em Bioquímica

Development of a theranostic system for central nervous system based on superparamagnetic nanoparticles

Dissertação para obtenção do Grau de Mestre em Bioquímica

Orientador: Professor Doutor Miguel Castanho, IMM FM/UL

Co – orientadores: Professor Doutor João Paulo Borges, DCM-FCT/UNL

Dr.ª Vera Luísa Santos Neves, IMM FM/UL

Jurí:

Presidente: Professor Doutor José Ricardo Ramos Franco Tavares
Arguente: Doutora Maria Manuela de Jesus Guilherme Gaspar
Vogais: Doutora Vera Luísa Santos Neves

FACULDADE DE CIÊNCIAS E TECNOLOGIA
UNIVERSIDADE NOVA DE LISBOA

October 2016

Mariana Filipa Mestre Pina Amaro
Licenciatura em Bioquímica

Development of a theranostic systems for central nervous systems based on superparamagnetic nanoparticles

Dissertação para obtenção do Grau de Mestre em
Bioquímica

Orientador: Professor Doutor Miguel Castanho, IMM FM, UL
Co-orientador: Professor Doutor João Paulo Borges, DCM-FCT/UNL
Doutora Vera Luísa Santos Neves, IMM FM, UL

Jurí:

Presidente: Professor Doutor José Ricardo Ramos Franco Tavares
Arguente: Doutora Maria Manuela de Jesus Guilherme Gaspar
Vogais: Doutora Vera Luísa Santos Neves, IMM FM, UL

October 2016

Development of a theranostic systems for central nervous systems based on superparamagnetic nanoparticles

"Never give up on a dream just because of the time it will take to accomplish it. The time will pass anyway."

Earl Nightingale

Acknowledgements

Quando pensei em fazer o mestrado em bioquímica não pensei que as coisas fossem sempre fáceis, mas houve alturas em que foram particularmente mais difíceis e não me querendo alongar tenho de agradecer a todos (ou quase) que de um modo ou de outro me ajudaram. É uma tarefa difícil pois encontrei bons colegas e, sem dúvida, bons amigos!

Em primeiro lugar, quero agradecer aos meus orientadores: Prof. Miguel Castanho, pela oportunidade em fazer parte do seu grupo de investigação, ao Prof. João Paulo Borges por ter acreditado em mim e por me ter dito algumas palavras sábias que me encorajavam e me ajudavam a não desistir.

À Dr.ª Vera Neves, pelo incansável apoio, suporte e orientação ao longo de todo o trabalho. Foi um prazer poder estar ao teu lado. Obrigada!

À Dr.ª Paula Soares, que mesmo não estando envolvida no meu trabalho nunca me faltou a tua ajuda, o teu apoio, a tua amizade e quando as coisas nem sempre pareciam ser fáceis tu ajudavas a que parecesse mais simples!

Ao Dr. Cesar Laia, pela ajuda que sempre se prontificou a dar, pela sua partilha sábia de conhecimento e pelo apoio!

Ao Prof. Jorge Silva, por se ter prontificado a ajudar-me com a microscopia de fluorescência.

À Coro, Susete e Ana Baptista, obrigada pelo vosso apoio e pela vossa boa energia! É um prazer estar com vocês!

À Tânia Vieira, obrigada colega! Tu estiveste sempre ao meu lado e daqui fica a nossa amizade para a vida!

Aos meus colegas de laboratório da FCT-UNL: Ana Almeida, João, Carlos, Gabi, Ana e Jaime! Vocês foram uns verdadeiros colegas de trabalho e boa disposição.

À Augusta, que alegrava os nossos dias com a sua boa disposição e tinha sempre uma palavra de amiga para dar. Obrigada!

Maïssa, you are a good friend. Thank you very much for all your help and your support from the begging! I will always wait for your visit!

Aos meus colegas de laboratório do IMM: Susana, Iris e Marco obrigada por terem recebido e sempre me ter sentido "em casa" na vossa companhia. Nuno, Filipa e Tiago, obrigada por me de uma maneira ou de outra me terem ajudado quando foi preciso.

À Rute, obrigada pela ajuda e pela partilha de conhecimento e de tarefas.

À Liliana, por toda a ajuda e partilha de conhecimento no laboratório.

À Sara, mais do que partilha de trabalho e conhecimento, foi partilha de muitos momentos que nem sempre foram bons, mas a tua ajuda e tua boa disposição tornava as coisas fáceis. Fica a nossa amizade para a vida! Obrigada!

Aos meus amigos, à Fi, ao Nani, à Mary e à Marta! Vocês são os maiores e melhores do mundo!! ☺

À minha família (aos meus pais, à minha irmã, meu "irmão" João e à minha Tia Carolina), por sempre me terem encorajado, me terem apoiado incondicionalmente e por perceberem mesmo quando a minha ausência se fazia sentir e mesmo assim compreenderem. Ao meu Salvador, que é pequenino e quando as saudades são muitas tenta lidar com elas à maneira dele! És o melhor do meu mundo! Estas palavras seguramente não chegam para agradecer e dizer o quanto foram e são importantes.

A minha nova família Travassos Leandro, que sempre me trataram com muito amor e foram um apoio muito importante! Obrigada!

E por fim, mas não menos importante, ao meu namorado, marido, amigo, companheiro João. Obrigada, obrigada por sempre me teres apoiado, ajudado, compreendido e teres sido sempre a melhor pessoa com quem se pode partilhar o mundo, a vida!

O trabalho apresentado está no âmbito do projeto TRANSDRUG (PTDC/BBBNAN/1578/2014) financiado pela Fundação para a Ciência e Tecnologia (FCT).

This work is funded by FEDER funds through the COMPETE 2020 Program and National Funds through FCT - Portuguese Foundation for Science and Technology under the project number POCI-01-0145-FEDER-007688, Reference UID/CTM/50025.

Resumo

A nanotecnologia tem revelado um enorme potencial na área da biomedicina com uma contribuição fundamental na área dos agentes de contraste para ressonância magnética de imagem ou no desenvolvimento de sistemas de libertação controlada de fármacos. Diversos estudos têm demonstrado que o efeito de alguns fármacos pode ser potenciado quando ligados a nanopartículas (NPs). Uma abordagem semelhante poderá ser relevante para o tratamento de doenças do sistema nervoso central (CNS).

Nos últimos anos, o conhecimento cérebro tem sido aprofundado e o consequente avanço da tecnologia tem levado a diversas aplicações biomédicas para o tratamento de várias doenças. No entanto, doenças como a de Alzheimer, Parkinson ou cancro continuam a ter uma taxa de mortalidade elevada e poucos tratamentos disponíveis. Na realidade, existem muitas moléculas com fins terapêuticos para estas doenças, mas mais de 98% das pequenas moléculas, e ~100% de proteínas, não conseguem atravessar a barreira hematoencefálica (BBB) e chegar ao CNS. A BBB é constituída por células endoteliais que estão alinhadas com os capilares de modo a prevenir a passagens de substâncias indesejadas do sangue para o tecido nervoso. Uma abordagem para ultrapassar esta dificuldade seria encontrar um sistema de libertação controlada capaz de levar o fármaco até à área afetada. Contudo, sistemas como estes podem afetar o correto funcionamento da BBB. Assim, o desenvolvimento de péptidos com capacidade de translocação pode ser um método alternativo. Estes péptidos translocadores de membrana (CPP) têm a capacidade de atravessar para o interior das células com várias moléculas a eles ligadas, por exemplo, fármacos com baixo peso molecular, lipossomas, anticorpos e NPs. Estes péptidos são degradados em compostos não tóxicos, têm baixo potencial para interações fármaco-fármaco e baixa probabilidade para causar reações imunológicas, quando comparados com proteínas.

A doença de Alzheimer é caracterizada por uma acumulação de proteínas insolúveis, como β-amiloides (Aβ), placas senis (SP) ou novelos neurofibrilares (NFT). Esta acumulação, leva à perda de sinapses e resulta em neurodegeneração, conduzindo a uma perda de memória e declínio cognitivo.

No presente trabalho, foram utilizadas nanopartículas de óxido de ferro duplamente funcionalizadas com pequenos CPP e anticorpo contra Aβ. O sistema tem a vantagem de poder funcionar como um sistema de teragnóstico, usando como mais-valia as propriedades magnéticas das NPs.

As NPs foram caracterizadas por várias técnicas em diferentes fases do trabalho e do processo de funcionalização. Foram obtidas partículas com estrutura cubica cristalina simples caracterizada por difração de raio-X, um tamanho médio de 9 nm obtido por microscopia eletrónica de transmissão, e um tamanho hidrodinâmico de 32.4 ± 2.1 nm para as SPIONs revestidas por acido dimercaptosuccínico (DMSA), obtido por dispersão dinâmica da luz. De modo a simular a BBB, foram utilizados sistemas *transwell in vitro* para estudar a transmigração celular das NPs funcionalizadas. Foi possível observar após 6 h, 23.7 ± 3.7% das SPIONs funcionalizas com o péptido foram capazes de translocar a BBB. As

NPs funcionalizadas com anticorpo e o péptido CPP são capazes de diminuir a agregação dos péptidos Aβ, quando comparado com um inibidor conhecido (morin).

Palavras-chave: Nanopartículas, barreira hematoencefálica, péptidos translocadores de membrana, anticorpos, inibidor de β-amiloide, doença de Alzheimer

Abstract

Nanotechnology has revealed its potential in the biomedicine area with fundamental contributions to the imaging contrast agents field or to drug delivery systems development. Several studies have shown that the effect of drugs could be improved when linked to nanoparticles (NPs). A similar approach may be relevant to the treatment of central nervous system (CNS) diseases. In the last decades the knowledge of the brain has increased and the advance in technology has led to several biomedical applications to treat human disorders. However, diseases such as Alzheimer's, Parkinson or cancer continue to be devastating and poorly treatable. There are several therapeutic molecules likely to treat these disorders, but more than 98% of all small molecules drugs, and ~100% of all large proteins are not able to cross the blood-brain-barrier (BBB) and get to the CNS.

The BBB is formed by endothelial cells that are aligned with the capillaries to prevent unwanted substances crossing from blood to nervous tissue. One approach to overtake this difficulty is to find a controlled delivery system able to supply the drug to the affected tissue. However, such systems have the potential to affect the correct BBB behavior. An alternative method is the use of peptides with translocation capacity. These cell penetrating peptides (CPPs) have capacity to translocate various types of cargo molecules to the cells interior, e.g. low molecular weight drugs, liposomes, antibodies and NPs. CPPs are degraded in non-toxic compounds, they have low potential to drug-drug interactions and low probability to cause immunologic reactions when compared with larger proteins.

Alzheimer's disease is characterized by an accumulation of insoluble protein as β-amyloid (Aβ), senile plaques (SP) and neurofibrillary tangles (NFT). The accumulation of these aggregates leads to a loss of synapses and neurodegeneration resulting in memory impairment and cognitive decline.

In the present work we have used iron oxide nanoparticles a dual functionalization, with a small peptide with translocation capacity and with therapeutic antibody against β-amyloid peptides. The system has the ability to function as a theranostic system by taking advantage of the magnetic properties of the nanoparticles. The nanoparticles were characterized by several techniques at different phases of the functionalization process.

The iron oxide nanoparticles revealed a simple cubic crystalline structure (by powder x-ray diffraction), a size of 9 nm (by transmission electron microscopy) and a hydrodynamic size of 32.4 ± 2.1 nm for the coated nanoparticles with dimercaptosuccinic acid (DMSA) (by dynamic light scattering). To mimic the BBB, a transwell *in vitro* system was used to study the translocation of functionalized nanoparticles across this barrier. After 6 h, 23.7 ± 3.7 % of functionalized nanoparticles were able to cross the BBB. In addition, to assess if the developed nanoparticle is able decrease or stop β-amyloid aggregation, the SensoLyte Thioflavin-T Beta-Amyloid (1-42) aggregation assay was used. It was found that functionalized iron oxide nanoparticles were able to inhibit β-amyloid aggregation when compared to a known inhibitor (morin).

Keywords: Nanoparticles, theranostic system, blood-brain-barrier, cell penetrating peptides, antibodies, β-amyloid inhibition, Alzheimer disease

TABLE OF CONTENTS

LIST OF FIGURES

LIST OF TABLES

ABBREVIATIONS

Aβ – Amyloid beta

AD – Alzheimer disease

APP – β-Amyloid precursor protein

ATR – Attenuated total reflectance

BBB – Blood Brain Barrier

BC – Bottom Chamber

CNS – Central Nervous System

CPP – Cell-penetrating peptides

DENV – Dengue virus capsid

DEN2C – Dengue virus type 2 capsid protein

dH_2O – Deionized water

DLS – Dynamic Light Scattering

DMEM – Dulbecco's Modified Eagle's Medium

DMSA – Dimercaptosuccinic acid

DMSO – Dimethyl sulfoxide

ECs – Endothelial Cells

EDC – 1-ethyl-3-(-3-dimethylaminopropyl) carbodiimide hydrochloride

EMA – European Medical Agency

FBS – Fetal Bovine Serum

FDA – Food and Drug Administration

FTIR – Fourier Transform Infrared Spectroscopy

GFP – Green Fluorescent Protein

IMAC – Immobilized Metal-Affinity Chromatography

IPTG – Isopropyl β-D-thiogalactoside

IONs – Iron oxide nanoparticles

MNPs – Magnetic nanoparticles

MRI – Magnetic Resonance Image

NHS – *N*-hydroxysuccinimide

NFT – Neurofibrillary tangle

NPs – Nanoparticles

OD – Optical Density

PET – Positron Emission Tomography

SP – Senile Plaques

SPIONs – Superparamagnetic Iron Oxide Nanoparticles

TEM – Transmission electron microscopy

TJs – Tight Junctions

UC – Upper Chamber

XRD – X-ray diffraction

Part I

General Introduction

1. ALZHEIMER'S DISEASE

In 1906, Alois Alzheimer discovered for the first time a form of dementia that became known as Alzheimer disease (AD). It is estimated that exists 48 million people worldwide affected with this neurodegenerative disease. AD is the most prevalent neurodegenerative disorder and the major cause of dementia related with ageing and affects specially patients with 65 years old or older when the clinical symphtoms start to manifest (Fig. 1.1). AD is characterized by an accumulation of insoluble protein aggregates such as β-amyloid (Aβ), senile plaques (SP) and neurofibrillary tangles (NFT). The molecular and cellular mechanisms responsible for the formation of these lesions are still unclear, with some controversy if the lesions are the first cause of the disease. The accumulation of aggregates leads to a loss of synapses and neurodegeneration and thus resulting in memory impairment and other cognitive problems (Maurer *et al.* 1997; Martin *et al.* 2013; Weiner *et al.* 2013; Nordberg 2015).

The common symptom in AD is a progressive decline in brain functions, loss of memory, comprehension and thinking consequently impairing personal activities of daily living (Holmes *et al.* 2004; Weiner *et al.* 2013; Wilhelm and Krizbai 2014; Daneschvar *et al.* 2015).

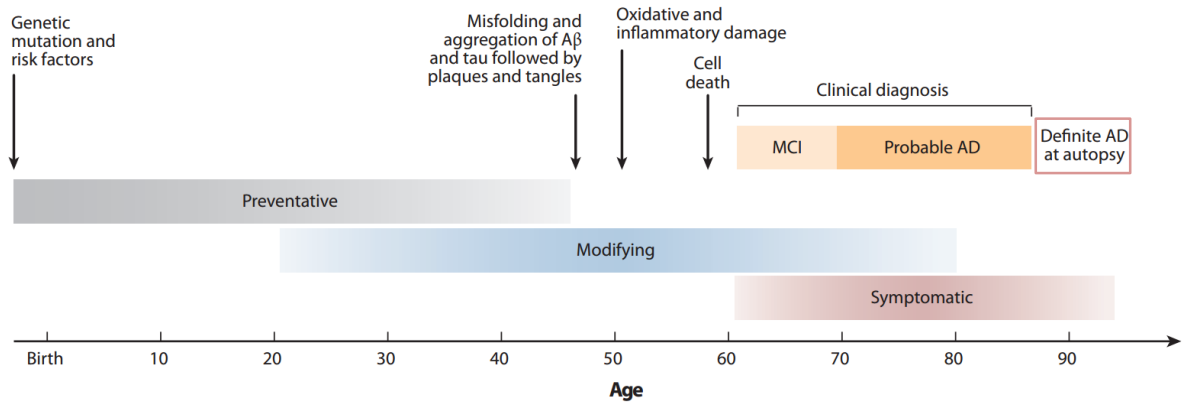

Figure 1.1. A possible timeline for progression and clinical symptoms in Alzheimer's disease (AD). The theoretical timeline progression for AD neuropathology and clinical changes. The gray (preventative), blue (disease modifying) and brown (symptomatic) bars shows time points at which different types of potential interventions may occur. MCI, mild cognitive impairment. Adapted from (Risacher and Saykin 2013).

1.2. β- AMYLOID HYPOTHESIS

The accumulation of misfolded proteins and different species of aggregates, is a common feature in neurodegenerative diseases (Meyer-Luehmann *et al.* 2006). In AD, the most prevalent aggregates in brain tissue (Aβ, NFT and SP) can appear intracellularly (oligomeric Aβ) and extracellularly (fibrillar Aβ plaques) (Wisniewski and Frangione 1996; Meyer-Luehmann *et al.* 2006; Murphy and LeVine 2010; Wyss-Coray and Rogers 2012; Lu *et al.* 2013; Heppner *et al.* 2015).

The reason for the formation of these aggregates is not completely clear but there is one theory in particular that has become the most relevant – the amyloid hypothesis (Reitz 2012; Giacobini and Gold 2013). The amyloid hypothesis predicts that 42 amino acids that forms Aβ ($A\beta_{42}$) are toxic, and when there is an overproduction or reduced clearance of this form from the brain, they became prejudicial. $A\beta_{42}$ monomers self-associates in different numbers, producing oligomers and fibrils (Fig. 1.2). This aggregation leads to a cascade of neurobiological events: inflammatory responses; aggregation and phosphorylation of Tau protein and other changes at neuronal level that ultimately leads to neurodegeneration and dementia (Sisodia and St George-Hyslop 2002; Zhang *et al.* 2011; Lee and Hyeon 2012; Reiman 2016).

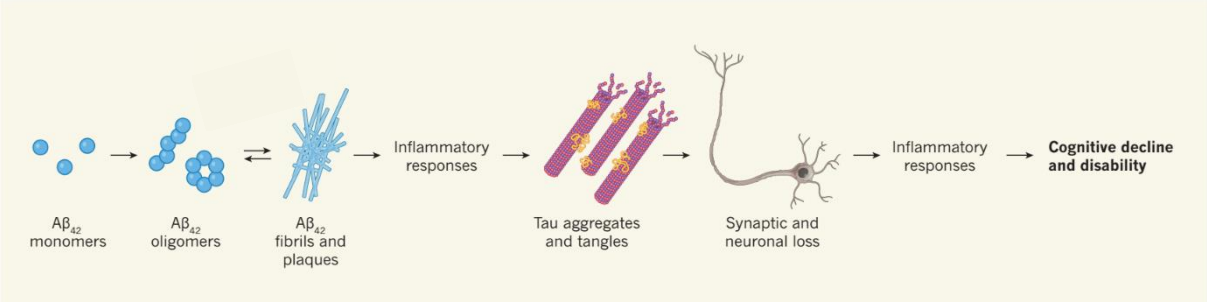

Figure 1.2. The amyloid hypothesis. The increasing of amyloid-β 42 (Aβ42) protein levels leads to a cascade of events in brain and consequently to Alzheimer's disease. This hypothesis predicts that Aβ42 monomers aggregate into damaging oligomers, fibrils and plaques. These aggregates cause an inflammatory response in the brain. The formation of Tau aggregates and tangles is not completely understood but the consequence is a synaptic and neuronal loss with a concomitant cognitive decline and disability. Adapted from (Reiman 2016).

The Aβ aggregates are derived by proteolytic cleavage from the amyloid precursor protein (APP). APP is a membrane protein with a large extracellular domain and a short cytoplasmatic domain. The full-length APP is sequentially processed by three proteases: α-, β- and γ-secretases (Fig. 1.3).

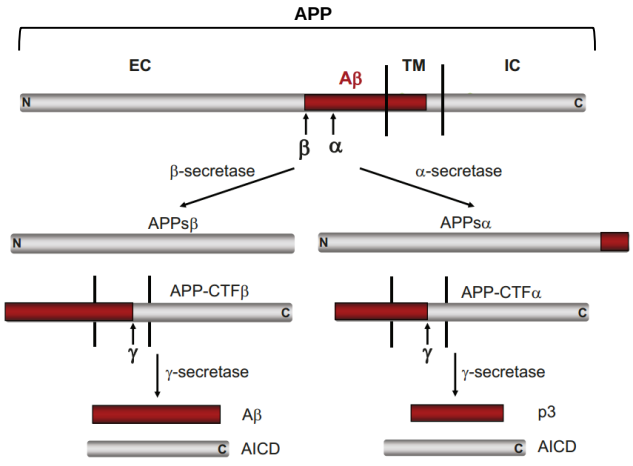

Figure 1.3. Amyloid precursor protein processing (APP). βA – β-Amyloid domain (red); EC – extracellular domain; TM – transmembrane domain; IC – intracellular domain; APPsα and APPsβ – APP derivatives; APP-

CTFα or APP-CTFβ membrane-tethered α- or β-carboxyl-terminal fragments; AICD – APP intracellular domain; N – N-terminal; C – C-terminal. Adapted from (Zheng and Koo 2011).

The cleavage of APP by α – secretase or β – secretase at the extracellular domain of the protein results in soluble APP derivatives (APPsα and APPs β) and the C-terminal domain of the protein remain bond to the membrane (APP-CTFα and APP-CTFβ, respectively). The γ–secretase cleaves within the transmembranar domain of the latter and leads to the generation of a 3 kDa peptide (p3, from cleavage of APP-CTFα) and Aβ (from cleavage of APP-CTFβ), plus the APP intracellular domain (AICD), in both cases (Zheng and Koo 2011).

The size of Aβ peptides can vary widely depending on the type of secretase (β and γ). The most abundant β–secretase is BACE1 (β–site APP cleaving enzyme 1) and their cleavage generates the N-terminal of Aβ. There are two others alternatives: BACE (β') that cleavage following the amino acid glutamic acid (Glu) at position +11 of the Aβ peptide and a BACE2 homolog which does not appear to cleave near the α–secretase site. The γ–secretase is a complex formed by four proteins (presenilin 1 or 2 (PS), nicastrin, anterior pharynx defective (APH1) and presenilin enhancer (PEN2)). Due to an imprecise cleavage of the enzymatic complex, the APP domain can have C-terminal truncated peptides endings between amino acids 37 to 43. The Aβ species ending with alanine at position 42 (Aβ 1-42) have a stronger propensity to aggregate comparing with Aβ 1-40 (Zheng and Koo 2011; Kummer and Heneka 2014).

The amyloid cascade is the primary hypothesis to explain the pathogenesis of AD, although there are several hypotheses proposed. The Tau hypothesis suggests hyperphosphorylation of tau protein as the primary pathogenesis event; the cholinergic hypothesis suggest that there is a decreased in the activity of choline acetyltransferase and acetylcholine levels in areas such as the cerebral cortex; the mitochondrial cascade hypothesis advocates the impairment of brain mitochondria as the first pathogenic event leading to neurodegeneration; the metabolic hypothesis suggests that the AD is caused by several changes in metabolic related processes (obesity, diabetes and hypercholesterolemia); and finally the vascular hypothesis presents the reduction of cerebral blood flow as the main characteristic (Mendiola-Precoma *et al.* 2016).

1.3. Diagnosis of Alzheimer's Disease

Early detection and diagnosis of a neurodegenerative disorder should be the first line action to prevent unwanted impairment (Frisoni *et al.* 2010; Assoc 2011). At the moment, the diagnostic for AD consists in a series of proceedings including mini-mental state examination (MMSE), cerebrospinal fluid (CSF) assays to measure the tau and Aβ proteins, magnetic resonance imaging (MRI) for brain volume and positron emission tomography (PET) scans to detect the presence of Aβ plaques. Although, the

definitive diagnosis still needs histopathological confirmation, the inaccessibility of the brain leads to the imaging has a major player in diagnosis of CNS diseases (Herholz *et al.* 2007; Johnson *et al.* 2012) (Johnson *et al.* 2012).

There are several contrast agents for PET approved by Food and Drug Administration (FDA) and European Medical Agency (EMA) although these agents are radioactive. Therefore there are an emergency to develop a novel imaging approach or contrast agent sensitive to imaging of Aβ peptide or tau protein that could change the landscape for diagnosis of CNS related diseases by imaging (Albert *et al.* ; Yang *et al.* 2012; Nordberg 2015).

The urge to diagnose AD in early stages of the disease using a non-invasive approach has been a relevant point for researchers, and consequently MRI and PET are the most investigated approaches. There are several studies with different contrast agents to MRI, in particular the use of superparamagnetic iron oxide nanoparticles and the incorporation of gadolinium (Gd^{3+}) into peptides that bind to Aβ using a protector of ligands (Johnson *et al.* 2012; Matharu *et al.* 2015).

Comparing PET with MRI it is possible to highlight some disadvantages of PET such as, some individual plaques cannot be seen due to the relatively low resolution of PET because of the radionucleotides short half-life and occasionally some false-positives are assumed. In contrast, MRI has higher resolution and can resolve individual plaques and the used contrast agents are not radioactive (Lu *et al.* 2013; Matharu *et al.* 2015).

1.4. THERAPIES

The current therapies available to AD do not prevent or reverse the disease. These drugs are focused on the reduction of symptoms (Pérez *et al.* 2016; Sala Frigerio and De Strooper 2016). Most of them are associated with Aβ cascade hypothesis to restore Aβ homeostasis in the brain that is disturbed by alterations in the production and clearance of Aβ. Based on this hypothesis, four strategies have been investigated to reduce the levels of Aβ in the brain. Prevention or reduction of Aβ formation, by targeting proteolytic enzymes that mediate processing of APP (β and γ-secretase); removal of existing amyloid deposits through immunotherapy; prevention or reduction of Aβ aggregation; and the enhancement of Aβ clearance (Fig.1.4) (Giacobini and Gold 2013; Sala Frigerio and De Strooper 2016).

The efficiency of all therapies depends on the ability of the drug to cross the BBB. Despite the large number of drugs that had been developed or are in clinical trials, ~99.6% of them do not get to the CNS probably due to the permeability issues at the BBB (Cummings *et al.* 2014).

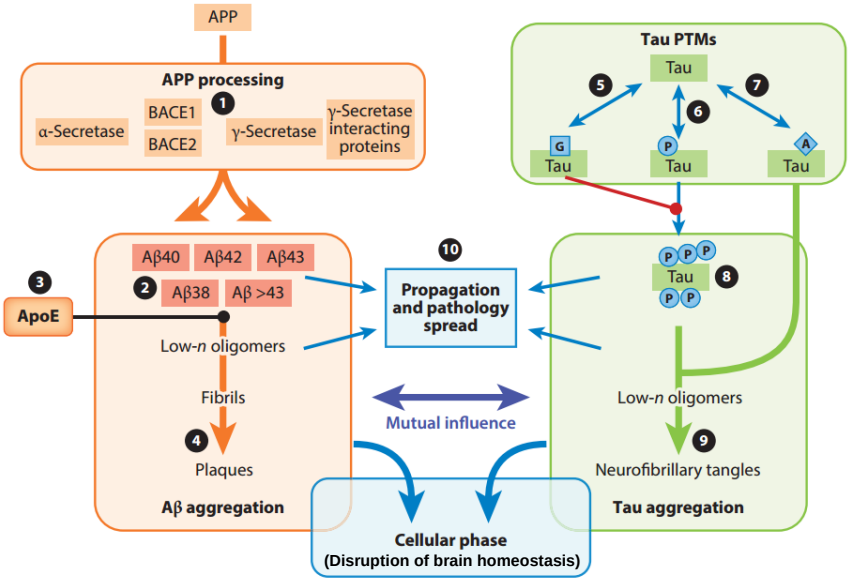

Figure 1.4. Targeting of the principal roots in Alzheimer's disease (AD) pathogenesis. The aggregation of β–amyloid (Aβ) may come from alterations in the different pathways/players involved in Aβ production or elimination. (1) Enzymatic activity modulation responsible for the amyloidogenic amyloid precursor protein (APP) cleavage is expected to decrease the production of Aβ monomers. (2) Molecules which bind Aβ monomers might prevent their further aggregation although, while the increase of the monomers degradation by introducing Aβ-degrading enzymes or favoring their clearance through (3) apolipoprotein E (ApoE) which can result in a decreased of the availability of monomers for further aggregation. (4) Small molecules and antibodies can bind to different species of Aβ aggregates should result in the decrease of synaptotoxic oligomers and should also enhance the clearance of aggregates from the brain by microglia uptake or peripheral sink mechanisms. Tau pathology occurs in parallel with Aβ pathology. This protein is extensively posttranslationally modified (PTM); the hyperphosphorylation is tau's main pathogenic modification. *O*-GlcNAcylation of tau (G-tau) opposes tau phosphorylation naturally; although inhibition of specific glycosidades could be beneficial. Strategies with the main objective to decrease phosphorylation (P-tau, (6)) and acetylation (A-tau, (7)) in order to reduce the production of proaggregating forms of tau. (8) Dephosphorylation of hyperphosphorylated tau to prevent further tau aggregation. (9) immunotherapy against tau aggregates could decrease or inhibit aggregation progression and may elicit their clearance. Aβ, tau monomers, and small aggregates can disperse over the brain and to be able to seed further aggregation at distal sites. (10) Prevention of spreading by immunotherapy or by targeting cellular mechanisms that facilitate the spreading that might prevent disease progression. APP – Amyloid precursor protein; PTMs, post-translational modifications; G, *O*-GlcNAcylation of tau; P, phosphorylation; A, acetylation. Adapted from (Sala Frigerio and De Strooper 2016).

1.4.1. IMMUNOTHERAPY

AD immunotherapy targeting Aβ has been recognized as one of the most promising approaches to treat AD. Antibodies have shown capacity as therapeutic agents, being highly selective and having the ability to treat many diseases, although their use in the brain is limited by the BBB (Liu *et al.* 2016; Neves *et al.* 2016).

Actually, it is possible to modify and/or design the antibodies using engineering to improve their therapeutic applications and translocation of the BBB using the natural entrances of the brain. In the past decades, extensive research in immunotherapy using monoclonal antibodies has revealed a great potential in inhibit or clearing the formation of Aβ species. This approach can break the amyloid cascade, halt neurodegeneration progress and prevent further reduction in cognitive and physical function (Giacobini and Gold 2013; Liu *et al.* 2016; Neves *et al.* 2016).

New strategies are being developed using monoclonal antibodies with conformation-specific anti-Aβ to recognize epitopes related to the conformational structure of Aβ aggregates, as well as epitopes based on the primary sequence of Aβ peptides (Fig. 1.5) (Liu *et al.* 2016).

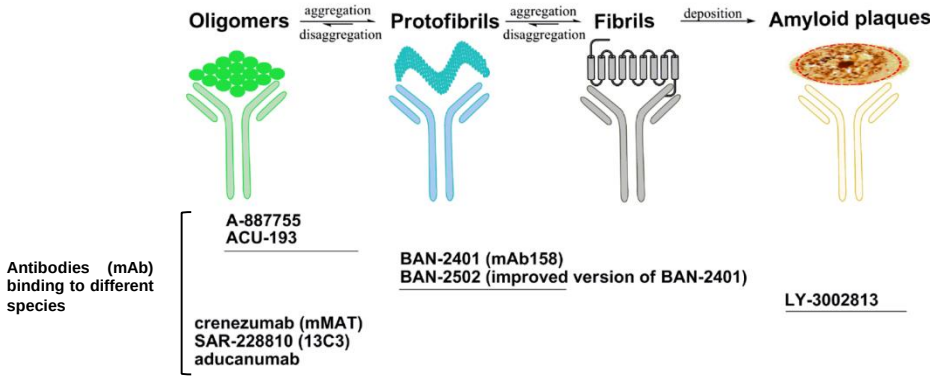

Figure 1.5. Antibodies to recognize different Aβ aggregate species. The solid line under each conformation represents the corresponding Aβ aggregate that the antibody is able to recognize. *Aβ* – amyloid-β; *mAb* – monoclonal antibody. Adapted from (Liu *et al.* 2016).

A recent study using an antibody (aducanumab) which binds to the Aβ aggregates has demonstrated to reduce brain levels of Aβ and it is already in phase III clinical program (Sevigny *et al.* 2016).

1.5. BLOOD BRAIN BARRIER

The main problem of treating CNS disorders is not due to the lack of molecules abbe to treat the disease but their ability to cross the BBB. From all developed molecules, ~98% of small molecules and ~100% of large molecules are not capable to get into CNS. For this reason, the development of drug

delivery system able to cross the BBB and that is be able to perform its function is an emergent target(Pardridge 2005; de Boer and Gaillard 2007).

The BBB is a multicellular vascular structure that separates the CNS from the peripheral blood circulation. This barrier is formed by endothelial cells (ECs) that are tightly connected to each other by tight junctions (TJ), astrocytes and pericytes (Fig. 1.6). At the molecular level, there are transporters and receptors which regulate what is able to across the BBB (Wolburg and Lippoldt 2002; Cecchelli *et al.* 2007; Banks and Erickson 2010; Obermeier *et al.* 2013; Neves *et al.* 2016).

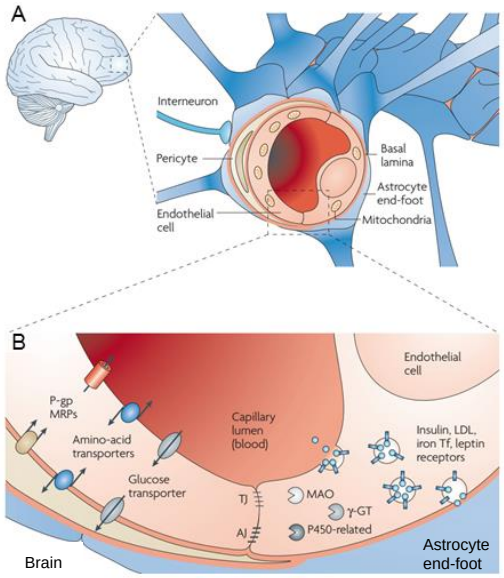

Figure 1.6. The Blood Brain Barrier. *A*, The BBB is formed by endothelial cells that interact with perivascular elements (basal lamina, closely associated astrocytic end-feet processes, perivascular neurons (represented by interneuron) and pericytes) to form a functional BBB. *B*, Cerebral endothelial cells form tight junctions produced by the interactions of several transmembrane proteins that effectively seal the paracellular pathway. These complex make the brain protect and practically inaccessible. Adapted from (Cecchelli *et al.* 2007).

The main function of this barrier is to maintain brain homeostasis, regulation of influx and efflux and transport and protection from any harmful substances. BBB is known as a dual role: first, it is a barrier for cells and solutes, and on the other hand, is selective to transport various substances, essential nutrients to the brain and potentially harmful metabolic products to the blood (Deguchi 2002).

In the last years, some strategies to cross the BBB have been developed to delivery therapeutic molecules to the brain but the ideal method should be controlled and should not damage the integrity of the BBB. Molecules such as glucose, amino acids and nucleosides can be transported into the brain through the endogenous BBB transporters, receptor-mediated transport (RMT). To find a new system capable to overcome the BBB is necessary to develop a drug delivery system able to translocate the BBB via endogenous BBB transporters (carrier-mediated transport (CMT), active efflux transport (AET) or receptor-mediated transport (RMT)) or as an alternative they can use the adsorptive-mediated transcytosis (AMT).

CMT and AET are responsible for the transport of small molecules (such as glucose, amino acids and nucleosides) between blood and the brain and the RMT is responsible for the transport across the BBB of specific endogenous large molecules (such as insulin, low-density lipoprotein (LDL) or transferrin). AMT is usually induced by electrostatic interaction of cationic proteins with endothelial cells (Neves *et al.* 2016).

1.6. CELL PENETRATING PEPTIDE (CPP)

Peptides are responsible for the regulation of many physiological processes. They are being used as a therapeutic agent in areas such as neurology, endocrinology and hematology (Santos *et al.* 2012).

The cell penetrating peptides (CPP) are short peptides (5 – 40 amino acids in length) with ability to achieve the access to the cell interior. The uptake mechanisms by which CPP enter in the cells are not completely understood but there are two principal uptake mechanisms, endocytosis and direct penetration. These CPP have the capacity to carry cargos such as peptides, protein, oligonucleotides and nanoparticles. They are positively-charged at physiological pH, usually, rich in lysine or arginine and due to their charges they are able to interact with the negatively-charged plasma membrane and the positively charged carrier (Sarko *et al.* 2010; Trabulo *et al.* 2010; Madani *et al.* 2011; Jafari *et al.* 2015).

The incessant search for effective and safe ways to transport compounds from the blood to the brain is imperative but it is extremely difficult not to interfere with BBB functions (Zou *et al.* 2013; Prades *et al.* 2015).

1.6.1. CPP FROM DENGUE VIRUS CAPSID PROTEIN

Dengue virus (DENV) is responsible for a variable spectrum of disease that ranges from an undifferentiated fever to dengue fever with potentially fatal dengue shock syndrome. DENV has a great capacity to delivery their DNA into the cells, resulting in an effective interaction with the cell membranes. The capsids of the DENV have been used to develop a CPPs using the capsids as a template (DENV C). The DENV C has four α-helical segments (α1, α2, α3 and α4) (Mairuhu *et al.* 2004; Freire *et al.* 2014).

The CPPs that adopt a specific secondary structure have higher stability with the membranes and promote their cellular uptake. Considering this fact, a CPP from the capsid protein of Dengue virus type 2 (DEN2C) from α–3 domain (pepH3 or pepA), was developed in order to be used as a shuttle in and out of the brain. A study revealed a great ability to cross the BBB returning to the blood circulation to be eliminated (Mairuhu *et al.* 2004; Eiriksdottir *et al.* 2010; Freire *et al.* 2014; Castanho *et al.* 2015).

2. MAGNETIC NANOPARTICLES

In the last decades, nanomaterials have been intensively investigated, with particular interest, in magnetic nanoparticles (MNPs). In particular, nanoparticles with 1 – 100 nm have been used in biomedicine as contrast agents in magnetic resonance imaging, cancer therapy, hyperthermia, tissue repair and drug delivery (Gupta and Gupta 2005; Lim *et al.* 2013b; Ruiz *et al.* 2014).

MNPs can be divided in paramagnetic, ferromagnetic and superparamagnetic particles. The impact of superparamagnetic and ferromagnetic particles on magnetic resonance imaging is similar. The composition of paramagnetic particles is different from the composition of superparamagnetic and ferromagnetic particles. Superparamagnetic and ferromagnetic particles have a magnetic core and a surface coating. The paramagnetic particles do not have an explicit magnetic core. Thus, their behavior on MRI is rather different from superparamagnetic and ferromagnetic particles (Rümenapp *et al.* 2012).

MNPs are usually formed by a mineral core of a magnetic mineral that could be iron, nickel, cobalt and their oxides, with an organic coating. From all iron oxide NPs, the most common biocompatible magnetic nanomaterials are pure oxides, magnetite (Fe_3O_4) and maghemite (γ-Fe_2O_3) (Gupta and Gupta 2005; Lim *et al.* 2013b; Ling and Hyeon 2013; Calero *et al.* 2014; Soares *et al.* 2014).

2.1. SUPERPARAMAGNETIC NANOPARTICLES

In last decades, superparamagnetic iron oxide nanoparticles (SPIONs) have gained a significant relevance. Iron oxide nanoparticles are designated by SPIONs when they are smaller than the critical size (< 15 nm) and consists of a single magnetic domain. In other words, these NPs exhibit a remarkably high MRI contrast effect, they are easily controlled by a magnetic external field and display a strong magnetic response even if subjected to a low magnetic field. For this reason, their movement in the blood can be controlled with external magnetic field and immobilized close to the targeted area (Fig. 1.7) (Faiyas *et al.* 2010; Busquets *et al.* 2014; Hola *et al.* 2015). SPIONs are commonly composed of magnetite (Fe_3O_4) and maghemite (γ–Fe_2O_3) cores (Laurent *et al.* 2008).

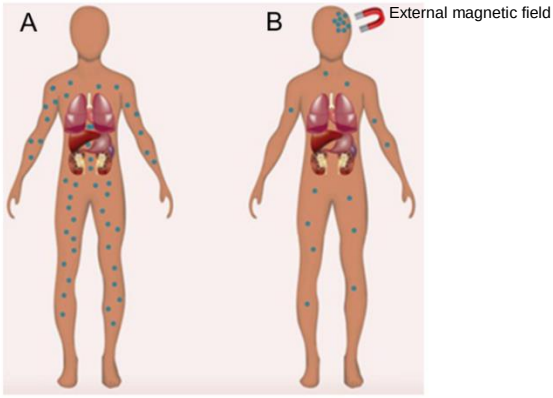

Figure 1.7. Application of an external magnetic field. *A,* No magnetic field applied and the iron oxide nanoparticles are in the blood circulation. *B,* External magnetic field is applied and the nanoparticles are immobilized to the target. Adapted from (Wu *et al.* 2015).

Despite the NPs being commonly used due to their natural elimination or their simple synthesis, there are some adverse reactions to avoid. When nanomaterials are exposed to biological systems, many undesirable reactions may occur. The generation of reactive oxygen species (ROS) upon exposure of cells is generally considered as a major contributor to the toxicity of naked iron oxide nanoparticles. For this reason, coating must be used to avoid this side effect (Tartaj et al. 2011; Ling and Hyeon 2013; Ruiz et al. 2014).

2.2. SYNTHESIS OF IRON OXIDE NANOPARTICLES

The synthesis methods can influence the NPs properties, such as size, dispersion of the particle-size and morphology. The most commonly precipitation method is chemical co-precipitation due to their extremely flexible method, and the surface properties controlled changing the experimental parameters (pH value, temperature and ionic strength). Using this option, the NPs are synthetized in water, which becomes an advantage for biomedical applications. There are several other options to synthetize NPs including microemulsions, sol-gel synthesis, hydrothermal reaction, hydrolysis and thermolysis of precursors (Hadj Farhat and Joubert 1984; Costa *et al.* 1994; López-Pérez *et al.* 1997; Wu *et al.* 2015).

Co-precipitation of ferric and ferrous ions in solution using a strong base leads to the formation of magnetite or maghemite (nucleation phase), depending up on the iron concentration, pH and the ratio of ferrous and ferric ions (Gnanaprakash *et al.* 2007).

2.3. Surface Modifications of SPIONs

The surface of SPIONs can be modified through the creation of atomic layers of some organic or inorganic molecules, which allows further functionalization by binding various bioactive molecules. However, more than the functionalization, it is the contribution of the coating to the NPs colloidal stability (Gupta and Gupta 2005).

Despite the fact that naked NPs are stable in high- and low- pH suspensions, but not in neutral pH, they must be coated for several reasons: increase the stability and protect SPIONs against aggregation, to protect the magnetic core against oxidation, to provide a reactive surface to allow their functionalization and, finally, to protect NPs against reticuloendothelial system (RES) uptake and elimination in order to enhance the blood circulation time and internalization efficiency (Laurent et al. 2008).

From all different polymers/molecules which can be used for coating NPs, meso-2,3-dimercaptosuccinic acid (DMSA) presents a great potential for target-drug delivery. This molecule binds to the nanoparticle through the carboxylate groups which establishes a negative surface charge of the particle and the thiol groups generates a "cage" of disulfide-cross-linked DMSA around the nanoparticle (Zhang et al. 2016).

Coated SPIONs with DMSA have been tested in vitro and in vivo, in particular their cell interaction process, pharmacokinetics and biodistribution in animal models with the main objective of drug delivery, NMR imaging and hyperthermia. (Ruiz *et al.* 2014).

2.4. Biomedical applications of SPIONs

When the physicochemical properties of SPIONs (size, composition and morphology) are combined with superparamagnetism, makes them highly promising candidates for many applications, such as drug delivery system, contrast agent in MRI and hyperthermia to cancer therapy. Due to their magnetic properties, they are commonly used as contrast agent in MRI (Laurent *et al.* 2008; Teja and Koh 2009; Ge *et al.* 2013).

Contrast agents are used to enhance the image obtained from MR. Some images obtained using a common contrast agent by magnetic resonance of soft tissues have a relatively high quality, although there are some cases where it is difficult to acquire sufficient image of contrast to diagnose the pathology of interest. In this case, SPIONs can be used to overcome this difficult. Actually, paramagnetic substances, such as gadolinium (Gd), have enhanced the magnetic resonance signal but the toxicity associated with them has led to a new focus of research in SPIONs (Li *et al.* 2013; Busquets *et al.* 2014; Hola *et al.* 2015).

A promisor strategy to treat AD has been studied to allow an early diagnosis, before clinical symptoms of the disease are manifested. The strategy involved the use of functionalized SPIONs with an antibody against Aβ1-42 to detect *in vivo* amyloid deposition by MRI (Andrieux and Couvreur 2013).

The functionalization of magnetic nanoparticles, or in particular, SPIONs allows to develop a theranostic system, using the magnetic properties for diagnostic through the MRI and therapy, using peptides, antibodies or therapeutic agent, in order words, NPs can be a promisor multifunctional platform (Fig. 1.8) (Lim *et al.* 2013a).

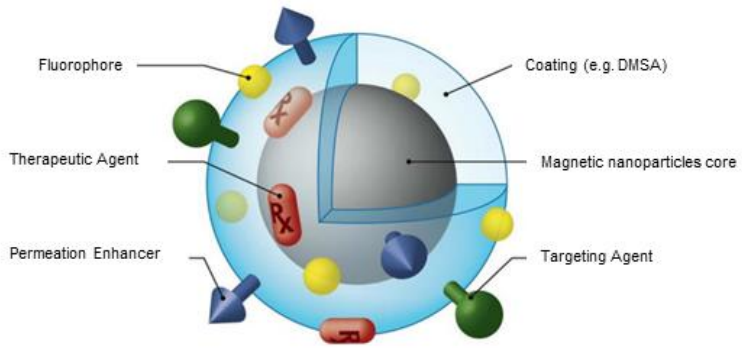

Figure 1.8. Multi functionalization of magnetic nanoparticles. Adapted from (Lim *et al.* 2013a)

2.5. DRUG DELIVERY AND A THERANOSTIC SYSTEM

In the last years, several drug delivery systems have been evaluated. The development of a successful drug delivery system with SPIONs as a vehicle, has to take in consideration the NPs shape, size and surface charge (Rümenapp *et al.* 2012; Ruiz *et al.* 2014).

The shape property has not been extensively studied so far, but some studies refer that rod-shaped and non-spherical nanoparticles showed a longer blood circulation time, when compared with spherical particles (Wahajuddin and Arora 2012).

Moreover, the size of the NPs determines their half-life in circulation. For instance, particles smaller than 10 nm are mainly removed by renal clearance, instead particles larger than 200 nm become concentrated in the spleen or can be taken up by phagocytic cells of the body leading to a decreased their plasma concentrations. However, NPs with 10 – 100 nm are considered to have an optimum size, with longer circulation times because they can easily escape the reticuloendothelial system in the body (Wahajuddin and Arora 2012; Andrieux and Couvreur 2013).

The NPs surface charge can provide some colloidal stability and determine their distribution in the body, thus affecting the NPs internalization in their target cells (Wahajuddin and Arora 2012).

More recently, a new strategy has been tried: formulations of theranostic systems, through the combination of diagnostic and therapeutic entities into one drug delivery vehicle. This new strategy

could prevent, diagnose and treat some diseases and may be possible the development of a personalized medicine (Ruiz *et al.* 2014; Ryu *et al.* 2014).

A promising approach is the use of SPIONs to detect and treat lesions in neurodegenerative disease as AD, since nanoparticles are able to cross the BBB (Mejias *et al.* 2011).

Part II

Aims of the Study

Alzheimer's disease (AD) is an age related neurodegenerative disease affecting, approximately, 48 million people worldwide (2015). AD is an incurable disease and the approved therapies are only able to treat symptomatic symptoms that do not mitigate the course of the disease. Therefore, there is an urgent need to find new therapies to treat AD. Immunotherapy targeting amyloid-β (Aβ) is one of the most promising therapies to treat AD. The main obstacles are the requirement of the antibody to cross the blood-brain-barrier (BBB), in order to reach the Aβ deposits in the affected brain tissue. The immunotherapy combined with magnetic resonance imaging (MRI) could provide more effective treatment of AD.

The main goal of this project was the development of a theranostic (diagnostic and therapy) system combining: the therapeutic properties of Aβ antibody; with the translocation properties of a cell penetrating peptide (CPP) and; coupling with iron oxide nanoparticles as a contrast agent in MRI.

The work was divided in five main aims:

1. Synthesis of superparamagnetic iron oxide nanoparticles (SPIONs);
2. Surface modification to obtain stable SPIONs and to provide the chemistry for bio-conjugation;
3. Functionalization of SPIONs with a CPP and Aβ antibody;
4. Evaluation of the translocation capacity of the system in a cell based BBB model; and
5. Proof-of-concept: antibody functionalized nanoparticle in inhibition of Ab aggregation

Part III

Materials and Methods

3.1. SYNTHESIS OF SUPERPARAMAGNETIC IRON OXIDE NANOPARTICLES (SPIONS)

Iron oxide nanoparticles were synthesized using an adapted method from Soares *et al.* based on chemical co-precipitation of the iron species (Soares *et al.* 2014). Briefly, ferrous and ferric chlorides $FeCl_3.6H_2O$ and $FeCl_2.4H_2O$ (Sigma-Aldrich, USA) were dissolved in 10 and 2.5 mL of deionized water (dH_2O), respectively, in order to obtain 1 and 2 M solutions. 50 mL of dH_2O was added to the iron mixture to achieve a final molar ratio of 1:2 (Fe^{2+}:Fe^{3+}). The final solution was deaerated with bubbling N_2. Furthermore, 10 mL of NH_4OH 25% (Sigma-Aldrich, USA) was rapidly added under vigorous stirring during 5 min. The reaction was stopped with 60 mL of dH_2O and the superparamagnetic iron oxide nanoparticles (SPIONs) were washed five times with water.

3.1.1. SPECTROPHOTOMETRIC DETERMINATION OF IRON BY UV-VIS

Iron content in the SPIONs was measured using 1,10-phenantroline colorimetric method (Talelli *et al.* 2009; Soares *et al.* 2014). Briefly, 40 μL of diluted SPIONs suspension were added to 20 μL HCl 37% and incubated 1 h at room temperature. Afterwards, 100 μL of hydroxylamine (100 $mg.mL^{-1}$) (Sigma-Aldrich, USA) (previously prepared in 0.01 M HCl), 500 μL of 1,10-phenantroline monohydrate (3 mg/mL) (Sigma-Aldrich, USA) (previously prepared in 0.01 M HCl) and 1140 μL of 500 mM ammonium acetate buffer solution (Panreac, Spain) were added. All the samples were made in triplicates, and the absorbance was measured at 510 nm using a (PG Instruments model T90+) spectrophotometer.

The calibration curve (Appendix I) was prepared using ammonium iron (II) sulfate hexahydrate (Sigma-Aldrich, USA) to prepare a stock solution of 360 μg/mL of iron. Different concentrations of the standard were prepared (0.7, 1.4, 2.8, 7.1, 10.6, 14.2, 35.6, 71.2, 106.8, 142.4, 178.0 and 213.6 μg/mL) and analyzed following the procedure described above.

3.1.2. SPIONS OXIDATION AND SURFACE MODIFICATION WITH DMSA

Dimercaptosuccinic acid (DMSA) was selected as a coating since it allows high stability of the nanoparticles in aqueous media and free ligand groups for further biomolecule conjugation (Mejias *et al.* 2010). The surface modification with DMSA was adapted from Fauconnier *et al.* and Xie *et al.* (Fauconnier *et al.* 1997; Xie *et al.* 2011). A set of pilot experiments were designed in order to find stable NPs with sizes smaller than 200 nm. The first step was the generation of oxidized SPIONs as they are more stable in aqueous solutions.

Before coating the SPIONs with DMSA, the pH of the suspension was adjusted to pH 3 with nitric acid 65% (Merck, Germany) with agitation to oxidize the nanoparticles. The oxidized SPIONs were kept at room temperature. The obtained SPIONs were stable but they were difficult to separate using a magnet or by centrifugation, hampering the subsequent coating and functionalization steps. For this reason, another method to oxidize SPIONs was tried by increasing the temperature.

In other approach, after synthesis the SPIONs solution was heated to 60 ºC during 30 min under vigorous stirring. The temperature oxidized SPIONs were not so stable as the pH obtained counterparts and it was possible to observe a deposit on the bottom of the beaker (Gnanaprakash *et al.* 2007).

The selected condition to proceed was the pH 3 of the SPIONs suspension. DMSA (Sigma-Aldrich, USA) was added immediately at a 3 – 4 ratio of [Fe^{2+}]/DMSA (Fauconnier *et al.* 1997). Four different final concentrations of DMSA were tested: 0.1; 0.2; 0.3; 0.4 and 0.5 M. DMSA was dissolved in 10 mL of dH_2O and the pH adjusted to 5.5 with 0.1 M NaOH (CARLO ERBA Reagents, France) under vigorous stirring (Massart 1980; Fauconnier *et al.* 1997). The reaction of DMSA with SPIONs was performed in the ultrasound bath during 5 h.

3.2. SPIONS FUNCTIONALIZATION

Two molecules, EDC (1-ethyl-3-(3-dimethylaminopropyl) carbodiimide hydrochloride) and NHS (N-hydroxysuccinimide) were used to allow cross-linking to a biomolecule (i.e. a protein in this case). The use of both molecules improves the efficiency of the reaction and the creation of a dry-stable (amine-reactive) intermediate. EDC couples NHS to carboxyls (from DMSA), forming an NHS ester that is considerably more stable than using EDC alone, while allowing for efficient conjugation to primary amines at physiologic pH (Hermanson 2013).

2 mg of DMSA-SPIONs were incubated with 5 mg of EDC (Sigma-Aldrich, USA) and 5 mg of NHS (Sigma-Aldrich, USA) previously dissolved in 500 mM sodium acetate (Scharlau, Spain), during 20 min on an orbital shaker. The activated SPIONs were washed with dH_2O and separated using a magnet between each wash.

For method optimization, first assays were performed with GFP-pepA, followed by assays with the single-domain antibody and peptide A (sdAb-pepA). The procedure for both assays was similar. The protein was diluted in PBS to achieve a final concentration of 0.48 mg/mL in 200 μL and then was added to 2 mg of activated SPIONs and incubated during 18 h at room temperature. The resulting reaction was washed with PBS using an Amicon Ultra-30 Centrifugal Filter (Millipore, Germany) during 2 min, 4000 x*g*, 3–5 times. The functionalized SPIONs are designated SPIONS-GFP-pepA, SPIONs-pepA or SPIONs-sdAb-pepA.

3.3. CHARACTERIZATION

The SPIONs (uncoated, DMSA coated and functionalized) were characterized using different techniques. Complementary information was provided by each technique such as size, hydrodynamic size, morphology and composition.

3.3.1. TRANSMISSION ELECTRON MICROSCOPY

Transmission Electron Microscopy (TEM) is a powerful technique for material science. The microscope has a high energy beam of electrons that cross through a thin specimen (sample) and the interaction between the electrons and the atoms is used to observe sample morphology (Williams and Barry 1996).

Samples were prepared by dilution in water from the original stocks in order to obtain a final concentration of 0.2 μg/mL NPs. A diluted suspension of NPs was placed in a Kevlar 25 mesh grid for analysis. TEM images were obtained in a Hitachi H-8100 II with thermionic emission LaB6.

3.3.2. X-RAY DIFFRACTION

X-ray diffraction (XRD) is an analytical technique primarily used for phase identification of a crystalline material and can provide information about the unit cell dimension. The sample is illuminated with X-rays of a fixed wavelength and the characteristics X-ray diffraction pattern provides a "fingerprint" of the crystals present in the sample. The diffractogram (intensity as a function of the diffraction angles) is compared with a standard reference patterns. This fingerprints allow the identification of the crystalline form (Swanson 1972).

Samples were dried overnight at 90 ºC and the X-ray diffraction analysis was done in a X'Pert PRO MDP (PANalytical) X-ray diffractometer. The results were evaluated using X'Pert HighScore Plus and each peak was compared with a standard reference pattern.

3.3.3. FOURIER TRANSFORM INFRARED SPECTROSCOPY

Fourier Transform Infrared Spectroscopy (FTIR) allows the determination of the composition of a solid, a liquid or a gas by adsorption or emission spectrum. In this particular case, all the samples were powder after being dried in the oven over-night at 90 ºC and analyzed by FTIR Nicolet 6700 (Thermo Electron Corporation) with attenuated total reflectance (ATR) for analysis. FTIR allows to obtain an emission or an adsorption spectrum of the infrared radiation. The samples composition is determined by the analysis of the peaks corresponding to the vibration of the atoms of a molecule presents in the sample material. FTIR spectroscopy uses the interference of radiation between two beams to produce an interferogram. The latter is a signal produced as a function of the change of pathlengh between the two

beams. The two domains of distance and frequency are interconvertible by the mathematical method of *fourier-transformation* (Stuart 2004; Smith 2011).

For each transmission spectrum of the sample, a background acquisition was done to rule out any contamination from other compounds. FTIR was used to evaluate the chemical composition of uncoated, DMSA-coated and functionalized SPIONs.

3.3.4. FLUORESCENCE MICROSCOPY

Fluorescence microscopy can be used for the examination of biological specimens, fixed or alive, since this technique allows the selective and specific detection of molecules in small concentrations and low background effect by the use of a fluorophore. The principle of fluorescence is the excitation of fluorescent molecules and consequent photon absorption. When a molecule absorbs photons, electrons are excited to a higher energy level. When electrons are in an excited state they return to the ground-state, vibrational energy is lost, what results in a shifted emission spectrum to longer wavelength (Lichtman and Conchello 2005; Yuste 2005). The fluorescence is separated from excitation light using a dichroic mirror and appropriate filter. This filter, allows to exclude or transmitting selected wavelengths of light leading to an optimization of the fluorescence signal and the reduction of unwanted background (Lichtman and Conchello 2005; Yuste 2005).
Samples were analyzed using a Nikon TI fluorescence microscope.

3.3.5. DYNAMIC LIGHT SCATTERING

Dynamic light scattering (DLS) is one of the most popular methods to determine the hydrodynamic size of particles. Dynamic light scattering measures Brownian motion and relates this to the size of the particles (Fig. 3.1). The particles are constantly moving due to Brownian motion, i.e. the movement of particles due to the random collision with the other molecules of the liquid that surrounds the particle. An important aspect of Brownian motion for DLS is that small particles move quickly and large particles move more slowly. The particles are illuminated with a laser and the intensity fluctuations of the scattered light are analyzed. The relationship between the size of a particle and its speed due to Brownian motion is defined in the Stokes-Einstein equation (Malvern 2013). It is possible to compute the sphere size distribution and give a description of the particle's motion in the medium, measuring the diffusion coefficient of the particle and using the autocorrelation function (Goldburg 1999).

All the samples analyzed by DLS were diluted in filtered (0.2 μM) dH_2O, and prepared carefully to decrease external contaminants. The final concentration of iron in each sample was 0.2 μg/mL. The zeta potential of SPIONs was also measured. This parameter allows the study of colloidal stability by measuring nanoparticle charge when an electrical field is applied. The zeta potential over a large range of pH (2−11) was measured to determine the best condition. A Horiba SZ-100 was used to analyze the samples.

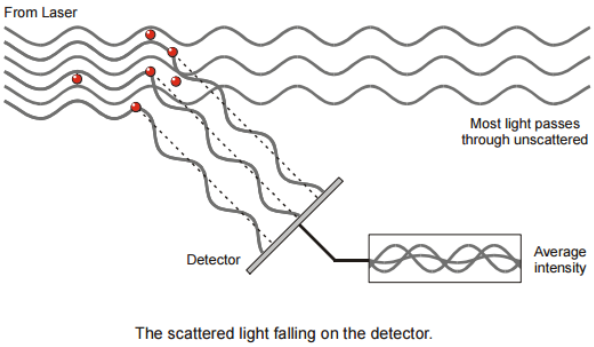

Figure 3.1. Particles are illuminated by a laser, and they will scatter the light in all directions. If a detector is located close to the particle, the detector will be illuminated by the scattered light. Adapted from (Malvern 2013).

3.4. Protein Expression and Purification

3.4.1. Protein Expression

The recombinant proteins were expressed using *Escherichia coli* BL21(DE3) cells. A selected clone was incubated in SB medium (3.2% peptone, 2% yeast extract, and 0.5% NaCl) containing kanamycin sulfate (50 µg/mL, Calbiochem, USA) at 37 °C, over-night with agitation. A 50 mL fresh supplemented SB medium with kanamycin was inoculated with 2 mL of the over-night culture. The bacterial culture was incubated at 37 ºC with agitation until an optical density (OD) of 0.6–0.7 at 600 nm was achieved. The proteins were induced using isopropyl-thio-*β*-D-galactoside (IPTG, Sigma-Aldrich, USA) to a final concentration of 0.6 mM and incubated in a shaking incubator for 6 hours at 37 ºC or overnight at 25 ºC. For recombinant proteins with GFP the incubation time was 6 h and for the sdAb was 16 h at 25 ºC. The cultures were centrifuged and the pellet stored at -20 ºC until used.

3.4.2. Protein Purification

The pellet was ressuspended in biding buffer (50 mM sodium phosphate, 1 M NaCl, 10% glycerol, pH 6.8) supplemented with anti-proteases (Complete EDTA-free proteases inhibition cocktail tablets, Roche, Germany) and 1 U/mL Benzonase Nuclease (purity >90%; Novagen, Denmark) to remove nucleic acids. The cells were lysed using the ultrasound tip during 2 min, 3 cycles with 50% pulsing at 4 ºC. The suspension was centrifuged and the supernatant was collected.

The proteins of interest (GFP-pepA, pepA and sdAb-pepA) have a HexaHistidine tag which enables its purification by immobilized metal-affinity chromatography (IMAC). A 5 mL His-column (GE Healthcare Life Sciences, Sweden) was equilibrated and the protein extract was injected following, washing and elution with elution buffer (50 mM Sodium phosphate, 1 M NaCl, 500 mM imidazole, 10%

glycerol, pH 6.8). With the purpose to obtain higher purity proteins, an additional step of gel filtration chromatography (Sephadex G-200, Sigma-Aldrich) was added.

The concentration of the protein in solution was determined through the Bradford assay. The methods consist in the addition of an acidic dye (Bradford Dye Reagent, BIO-RAD, Germany) and the measurement of the absorbance at 595 nm in a microplate reader. The absorbance of the sample when compared to a standard curve provides the protein concentration. The standard curve was obtained using bovine serum albumin (BSA, Sigma-Aldrich, USA) (Bradford 1976).

3.4.3. SDS-PAGE electrophoresis

The purity of the proteins can be analyzed using sodium dodecyl sulphate-polyacrylamide gel electrophoresis (SDS-PAGE). This type of electrophoresis uses two gels, a stacking and a running gel. The electrical current moves through the buffer and the SDS-coated negatively charged proteins migrate towards the anode. The polyacrylamide gel contains a stacking gel on top of resolving gel (Fig. 3.2). The stacking gel (4% acrylamide) contains larger pores than the resolving layer allowing the concentration of all proteins in a thin line before reaching the resolving gel. The running gel has a drastic difference in pore size, 12% acrylamide, and therefore in this gel the proteins will be separate according of their size (Hames 1998).

The stacking gel consists of 4% of acrylamide (30% acrylamide/bis solution, BIO-RAD, Germany), 0.15% SDS (OmniPur), TEMED (MERK, Germany) and 0.075% of APS (BIO-RAD, Germany), 0.1875 M Tris-HCl pH 6.8. The resolving gel consists of 12% acrylamide (30% acrylamide/bis solution, BIO-RAD, Germany), 0.1% SDS (OmniPur), TEMED (MERK, Germany), 0.05% of APS (BIO-RAD, Germany) and 0.378 M Tris-HCl 8.8. After gel polymerization and sample denaturation with β-mercaptoethanol (100% purity, Calbiochem, USA), SDS and 95 ºC/5 min, 10 µg of all proteins were applied per well, except for sdAb-pepA (6 µg). 5 µL of the protein ladder PageRuler Prestained Protein Ladder (Thermo Fisher Scientific, Lithuania, EU) was used. Finally, polyacrylamide gels were stained with Coomassie brilliant blue G-250 (BIO-RAD, UK).

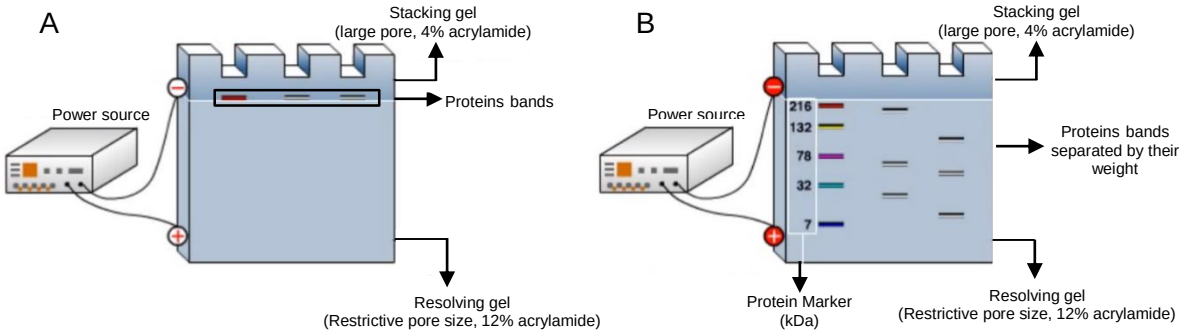

Figure 3.2. Scheme of SDS-PAGE system. *A*, Concentration of the proteins in the stacking gel. *B*, Migration and separation of the proteins in the resolving gel.

3.5. *IN VITRO* BBB MODEL

Cell-culture-based models have contributed for the knowledge of the blood-brain-barrier (BBB). The first *in vitro* model of BBB was established in 1973 and since then several models have been generated from human, bovine, rat, porcine and mouse cell lines (Nakagawa *et al.* 2009; Helms *et al.* 2014).

The BBB model intend to simulate the BBB with brain endothelial cells (BECs) culture growing on one side of a porous membrane positioned between two compartments, as it is shown in Fig. 3.3A (Muruganandam *et al.* 2002; Brown *et al.* 2007; Niewoehner *et al.* 2014). In the present study mouse brain endothelial cells bEnd.3 cells (ATCC 2299, American Type Culture Collection, Manassas, VA, USA) were used as a BBB model.

The bEnd.3 cells (passages 26-30) were cultured to achieve 80–90% of confluence in Dulbecco's Modified Eagle's Medium (DMEM) supplemented with 10% of fetal bovine serum (FBS) and 1% of Penicillin-Streptomycin (pen/strep), all from Gibco. For all the assays performed, polyethylene terephthalate (PET) membrane filter (1 µm pore size) was used in 24-well cell culture plates (BD Falcon, US). The maximum volume added was 200 and 500 µL to the upper chamber (UC) and bottom chamber (BC), respectively. Fibronectin (3 µg/mL per insert; CalBioChem®, Germany), a glycoprotein involved in various functions including cell adhesion, was added to the UC to allow the growth and consequent adhesion of the cells culture.

bEnd.3 cells (3000 cells per insert) were grown to reach a confluent monolayer after 11 days incubation at 37 ºC, 5% CO_2 in DMEM supplemented with FBS and pen/strep (Fig. 3.3B).

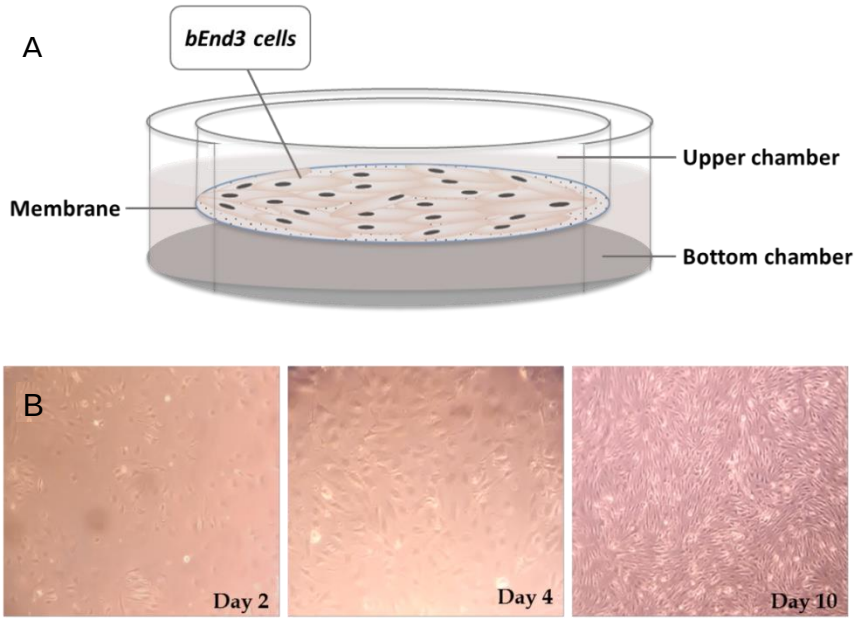

Figure 3.3. ***In vitro*** **BBB model.** *A*, The in vitro BBB model consists of a transwell system with an insert in which bEnd.3 cells are grown separating two chambers A. The insert, or apical side, corresponds to the blood side, while the base (bottom chamber) corresponds to the brain side. Peptides were added to the top compartment. *B*, bEnd.3 cells at 2, 4 and 10 days after culturing procedures.

3.5.1. In vitro transcytosis assay and Detection of recombinant GFP proteins by fluorescence

The first assays were made using GFP recombinant proteins (SPIONs-GFP-pepA) with the main goal of estimate the amount of translocated protein and its interaction with the cells membrane by simply using the fluorescence of the GFP (Green Fluorescent Protein).

Different incubation times were tested for both SPIONs-GFP and SPIONs-GFP-pepA. Initially different time points (30 min – 7 h) were tested.

6 µg/mL of SPIONs-GFP-pepA were added to the UC. The samples were diluted in DMEM without phenol red (Gibco, ThermoFisher, USA) supplemented with 10% of FBS. All the assays were performed using DMEM without phenol red medium. On the day of the assay, inserts were washed two times with PBS 1X, at 37 ºC, followed by three washes with DMEM without phenol red, at 37ºC. Then, the samples were added to the UC and incubated for 6 hours at 37 ºC, 5% CO_2. After 6h of incubation, the samples were collected to determine the apical and basolateral amount of protein. The content of recombinant GFP proteins in the samples were quantified by fluorescence detection using a black microplate 96 (Eppendorf AG, Hamburg, Germany) in Infinite M200 (TECAN) fluorescence reader, using 395 and 509 nm for the excitation and emission wavelengths, respectively.

After established the best conditions for the GFP fused proteins, the following step was to evaluate the SPIONs-pepA and SPIONS-sdAb-pepA. The time point of 6 h was chosen and the sample amount was 50 µg/mL of each protein.

3.5.2. DETECTION OF PROTEINS BY WESTERN BLOT

The collected samples from the translocation assay with SPIONs-pepA and SPIONS-sdAb-pepA were quantified by western blot, using an antibody against the His tag, present in both proteins.

First, samples were resolved by SDS-PAGE electrophoresis. 6 µL of UC and 15 µL of BC samples previously denatured with β-mercaptoethanol were applied onto the gel. In addition, 100 ng of sdAb-pepA and pepA control were added to the same gel.

The gel obtained from the SDS-PAGE electrophoresis was compressed with a solid nitrocellulose membrane (Amersham Protran 0.2 NC, GE Healthcare Life Sciences, Sweden) in a cassette and immersed in transfer buffer (20% of methanol) (BIO-RAD, Germany) between two parallel electrodes, forming a sandwich (Fig. 3.4). The transfer occurred at 250 mA, during 1 h, and the membrane was washed with dH_2O several times to remove methanol, and lastly, the protein bands were stained with Ponceau S solution (Sigma-Aldrich, USA) and washed several times with PBS 1x, 0.2% Tween (CalBioChem®, Germany).

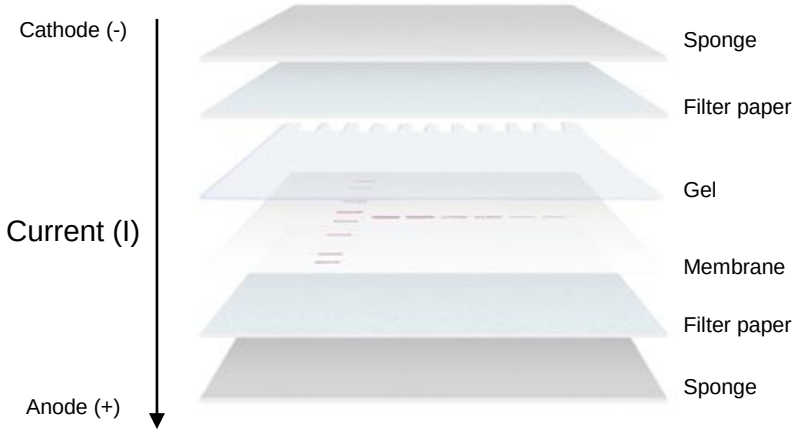

Figure 3.4. Western Blotting scheme. Transfer of proteins from SDS-PAGE gel to a nitrocellulose membrane. A transfer "sandwich" is assembled with the following layers in order, from cathode (-) to anode (+): sponge, filter paper, SDS-PAGE gel, nitrocellulose membrane, filter paper and sponge. Adapted from (BIO-RAD 2016).

Before incubation with the primary antibody, the membrane was incubated 1 h at RT with blocking buffer (5% nonfat milk in PBS 1x, 0.2% Tween) to prevent the nonspecific binding of the antibodies. Finally, the nitrocellulose membrane was incubated with 0.02 U/mL of a conjugate antibody (Anti-His6-HRPeroxidase, Roche, Germany) diluted in 1% nonfat milk in PBS 1x with 0.2% Tween for 1 h at RT with agitation.

For detection, the membrane was washed in PBS 1x to remove Tween and the ECL Prime solution (GE Healthcare Life Sciences, Buckinghamshire, UK) was added. The solution contains a

chemiluminescent substrate that emits light upon conversion by the peroxidase enzyme, which can be captured using a CCD camera-based imager (ChemiDoc™ XRS+, BIO-RAD, Germany).

3.5.3. *IN VITRO* INTEGRITY STUDIES

Following the *in vitro* transcytosis assays, bEnd.3 cells integrity was evaluated to determine the functionalized SPIONs toxicity. After washing the bEnd.3 cells two times with PBS 1x, and one time with DMEM without phenol red (Gibco), diluted FD40 solution (Sigma-Aldrich, USA) was added. FD40 solution was prepared from dilution of stock solution of 25 mg/mL to obtain a solution with absorbance lower than 0.1 (measured at 493 nm). Cells were incubated for 2 h with diluted FD40 and samples quantified by fluorescence detection using a black microplate 96/V (Eppendorf AG, Hamburg, Germany) in Infinite® M200 (TECAN) fluorescence reader using 493 and 560 nm, as the excitation and emission wavelength, respectively.

3.6. THIOFLAVIN-T FLUORESCENCE ASSAY

Thioflavin-T (ThT) is one of the most frequently used dyes for amyloid detection (Lindberg *et al.* 2015). Thioflavin-T is a cationic benzothiazole dye (Fig. 3.5A) that displays enhanced fluorescence upon binding to amyloid fibrils (Fig. 3.5B) (Biancalana and Koide 2010). ThT is a molecular rotor with short fluorescence lifetime and low quantum yield in water due to rapid dissipation of excitation energy through rotation around the central carbon bond. When bound to amyloid fibrils, in particular to the crossed-β structure, ThT rotation becomes constrained resulting in an increased quantum yield (Khurana *et al.* 2005; Biancalana and Koide 2010).

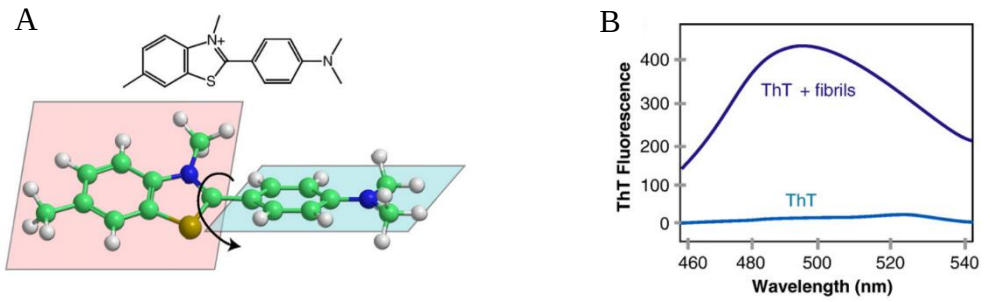

Figure 3.5. Thioflavin assay. *A,* Structure of ThT and rotation round the central carbon bond. *B,* Enhanced ThT fluorescence upon binding to amyloid fibrils. Adapted from (Lindberg et al. 2015).

Amyloid fibrils formed from different proteins share the common cross-β structure and are able to bind ThT. However, amyloid fibrils formed from different amyloid samples can differ significantly in their ability to enhance ThT emission. Nevertheless, ThT assay is a useful and standard method to

rapidly measure amyloid fibril formation and to screen for inhibitors able to inhibit the aggregation process.

The assay was performed with SensoLyte Thioflavin-T Beta-Amyloid (1-42) aggregation Kit (AnaSpec, Fremont, CA) according to manufacturer's protocol. Briefly, thioflavin-T (ThT) measurements were made by tacking ThT aliquots and diluting them in assay buffer (SensoLyte component A) to 200 μM ThT (final concentration). Test samples (sdAb, sdAb-pepA, SPIONs-sdAb, SPIONs-sdAb-pepA in PBS) were prepared in assay buffer containing 200 μM ThT, 46 μM Aβ42 and 3.7 μM sdAb, 8.7 μM sdAb-pepA, 1.6 μM SPIONs-sdAb and 1.5 μM SPIONs-sdAb-pepA, respectively. An inhibitor control was assayed containing ThT, Aβ42 and 100 μM of the supplied aggregation inhibitor morin in parallel with the positive control containing ThT and Aβ42 without inhibitor. A vehicle control (ThT and PBS), a test sample control (ThT and test sample) and a blank (ThT and assay buffer) were also performed.

Immediately after sample preparation, the fluorescence intensity was measured in a TECAN Infinite M200 (Männedorf, Switzerland) at 37°C using an excitation of 440 nm and emission of 484 nm, with 15 sec shaking between reads to facilitate aggregation. The fluorescence was followed 1.5h with measurements every 5 min. The fluorescence values were corrected by subtracting the background fluorescence of ThT in assay buffer.

Part IV

Results and Discussion

Alzheimer's disease is characterized by an accumulation of amyloid-β protein aggregates (Aβ oligomers and fibrils) in the brain tissue leading to an inflammatory response. From all current or under investigation therapies, the antibody therapeutic approach is a promising path to tackle this devastating disease. However, the main challenge for all therapies to the treatment of brain disorders is the permeability of the BBB. Its principal function is to control the exchange of substances between the blood and the fluids of the brain, imposing an obstacle to the treatment. This is true for either small molecules or protein-based therapies, as the one assessed in this work (Banks and Erickson 2010; Neves *et al.* 2016; Reiman 2016; Tycko 2016).

In the recent years, several strategies have been developed to delivery therapeutic molecules to the brain, such as the use of cell penetrating peptides (CPPs) with capacity to translocate various types of cargo molecules to interior of cells. Recently, CPP designed from an α-helical domain of the dengue virus capsid protein, pepH3, were studied and revealed a great ability to cross the BBB and return to the blood circulation to be eliminated (Freire *et al.* 2013; Corte-Real *et al.* 2016; Kristensen *et al.* 2016).

The goal of the work described was to further develop a BBB translocation system with a therapeutic and diagnostic entity. The translocation properties of CPP were combined with the therapeutic properties of an antibody anti β-amyloid into a delivery system amenable to magnetic resonance imaging. Superparamagnetic iron oxide nanoparticles (SPIONs) were selected to provide magnetic properties to the system. When iron oxide nanoparticles are below 20 nm, they have a single domain and became superparamagnetic acting as a "single super spin" with high magnetic susceptibility. When an external magnetic field is applied, the particles became magnetized until their saturation magnetization. Upon removal of external magnetic field, SPIONs lose their magnetism, a property that can be useful in biomedical applications (Wahajuddin and Arora 2012; Li *et al.* 2013; Santhosh and Ulrih 2013; Shevtsov *et al.* 2015).

SPIONs are usually employed as a contrast agent in magnetic resonance imaging with better properties than common gadolinium-based agents (Frisoni *et al.* 2010; Hola *et al.* 2015; Shevtsov *et al.* 2015). They might contribute to early detection of the β-amyloid in the affected brain tissue, when coupled to antibodies that recognize Aβ.

The work is divided in five parts: synthesis of SPIONs; surface modification; functionalization of SPIONs with all proteins tested (SPIONs-GFP, SPIONs-GFP-pepA, SPIONs-pepA and SPIONs-sdAb-pepA); evaluation of the system in a cell based BBB model and; assessment of the therapeutic properties of the antibody in the functionalized nanoparticle.

4.1. SYNTHESIS OF SPIONS

Magnetic oxides, specially magnetite (Fe_3O_4) and maghemite (γ-Fe_2O_3), have been intensively investigated because they are easy to be obtained and have properties that permit various applications (Zhang *et al.* 2009).

The synthesis of the iron oxides using the co-precipitation method is, perhaps, the simplest chemical approach to obtain magnetic NPs. This method is commonly used since usually produces NPs with 10 nm or less. Nevertheless, there are still some difficulties, mainly related to the control of NPs size, shape and morphology. These parameters can fluctuate with iron concentration salts, pH, temperature and stirring velocity during synthesis (Kim *et al.* 2001; Gnanaprakash *et al.* 2007; Laurent *et al.* 2008; Valenzuela *et al.* 2009).

The mechanism generally accepted of the Fe_3O_4 NPs formation using ferrous and ferric salts (with a ratio of 1:2) by co-precipitation method is represented by the equation below (Eq. 1) (Gupta and Gupta 2005; Faiyas *et al.* 2010):

$$Fe^{2+} + 2Fe^{3+} + 8OH^- \rightarrow Fe_3O_4 + 4H_2O \qquad \text{(Eq. 1)}$$

The NPs produced in this work were precipitated using ammonia, as a base, with a final pH 8 – 9. Bubbling with N_2 through the solution was used to protect the critical oxidation of the magnetite at this point and also to reduce particle size, when compared with methods without removing the oxygen during synthesis.

Independently of the SPIONs application, but specifically in biomedical field, it is crucial to have a colloidal stability of NPs to avoid aggregation (Soares *et al.* 2015). For this reason, at the beginning of this work two different conditions were tested in order to obtain maghemite, to maintain its favorable chemical and physical stability (Sun and Zeng 2002; Laurent *et al.* 2008; Teja and Koh 2009). Therefore, after synthesis, the NPs solution was either heated to ~100ºC (condition I) or pH was changed to pH 3 (condition II).

X-ray diffraction (XRD) was used to confirm which species were obtained for each condition. The spectra were compared with standard diffraction patterns of magnetite and maghemite, using the Match software (Fig. 4.1). The goal of this software is to obtain a list of peaks (2θ and intensity values) with highest possible precision in comparison with a reference pattern database (Putz 2003). Magnetite and maghemite are both considered to be ferromagnetic, and to have very similar identical crystalline structures and physical properties, so their identification by XRD can be difficult (Rebodos and Vikesland 2010).

In condition I (temperature), the results of XRD show the presence of both species, magnetite and maghemite (Fig. 4.1*A*) but with higher percentage of magnetiteg (73.9%). Their characteristic 2θ values are 30.35, 35.73, 43.48, 57.46 and 63.05 for maghemite and 30.58, 35.96, 43.78, 57.95 and 63.66 for

magnetite. In condition II (pH) (Fig. 4.1*B*) the prevalent species is magnetite (75.6%) with a lower percentage of maghemite (24.4%). Their characteristic 2θ values for magnetite are 30.32, 35.59, 43.28, 53.80, 57.14, and for the maghemite species the 2θ values are 62.86 and 30.12, 35.59, 43.25, 53.67, 57.28 and 62.28 (Appendix II).

The magnetite (Fe^{2+}) species is oxidized into the more stable maghemite (Fe^{3+}) during both processes (Rebodos and Vikesland 2010). However, the oxidation of the NPs by pH is less efficient when compared with oxidation by temperature.

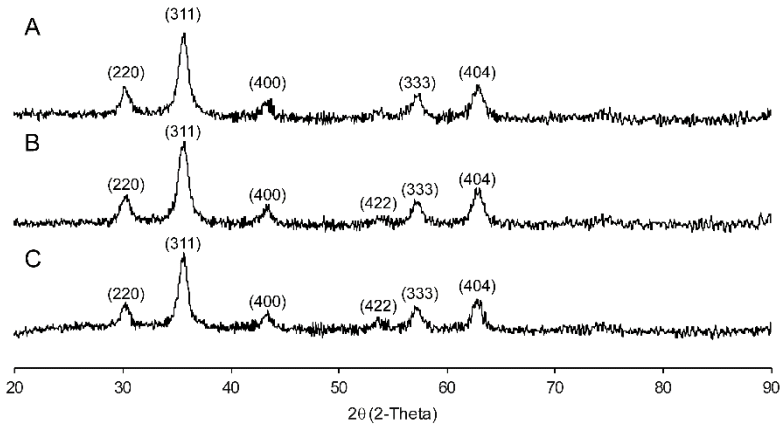

Figure 4.1. XRD of SPIONs oxidized by different conditions. *A*, SPIONs oxidized by temperature. *B*, SPIONs oxidized by acidic pH, 3. *C*, SPIONs oxidized by pH and surface modification with 0.3 M DMSA. The Miller indices (hkl) are represented in panel A.

The average grain size was calculated for naked NPs (condition I and II) and DMSA coated SPIONs using Scherrer's equation (Eq. 2), where τ is equivalent to the grain average core diameter, K is the grain shape factor (K = 0.94), λ is the incident x-ray wavelength, β denotes the full width at half-maximum (in radians) of the highest intensity and θ is the corresponding diffraction angle (2θ) (Soares *et al.* 2015).

$$\tau = \frac{K\lambda}{\beta \cos\theta} \qquad \text{(Eq. 2)}$$

The average grain obtained using equation 2, for naked SPIONs using condition I (2θ = 35.58) was 8.9 nm and using condition II (2θ = 35.53) was 8 nm, which indicates that the oxidation method does not change the average particle size of the NPs.

The purpose of using iron oxide NPs in this work is to explore their magnetic properties in magnetic resonance imaging, as a contrast agent. The magnetite has a higher magnetic saturation than maghemite

(Rebodos and Vikesland 2010). The higher stabilization of maghemite had to be balanced by the higher magnetic saturation of the magnetite species. The condition II was used during coating of the SPIONs (point 4.2) to obtain a stable NPs with good magnetic properties. There were no differences in the XRD results between the two conditions and as the subsequent DMSA coating process has to be carried out at pH 3, the condition II was selected.

4.2. SURFACE MODIFICATION WITH DMSA

The SPIONs were coated with dimercaptosuccinic acid (DMSA) (Fig. 4.2*A*) with two main purposes: provide colloidal stability over a large pH range (3 − 11) and provide the necessary chemistry for bio-conjugation.

DMSA binds to SPIONs through the carboxylate groups and the -SH groups surrounds the nanoparticle by forming disulfide bounds. The free -COOH and -SH groups allow the functionalization of the NPs with biomolecules (Fig. 4.2*B*) (Fauconnier *et al.* 1997; Garcia *et al.* 2005; Ruiz *et al.* 2014; Zhang *et al.* 2016).

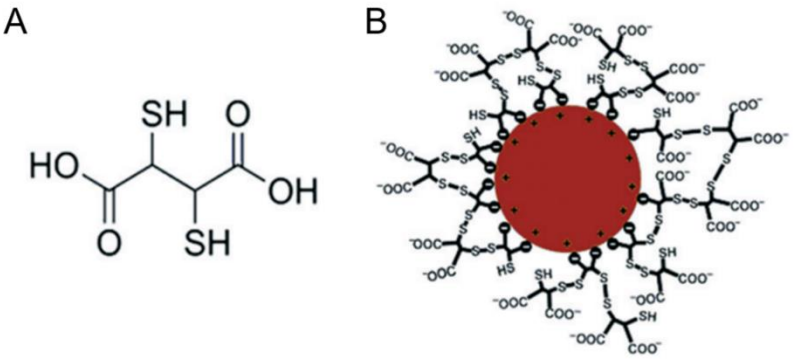

Figure 4.2. Dimercaptosuccinic acid (DMSA). *A*, structural formula of meso-2,3-dimercaptosuccinic acid. *B*, SPIONs coated with DMSA. From (Zhang et al. 2016).

Different DMSA concentrations (0.1 – 0.5 M) were tested to determine the best ratio of coating agent able to originate particles with small sizes and to avoid flocculation/aggregation (Fauconnier *et al.* 1997).

The hydrodynamic size of the nanoparticles was evaluated by dynamic light scattering (DLS) (Table 4.1). For all the tested conditions the particle size was very similar around 32 – 37 nm and the polydispersity index (PDI) was in an acceptable range, except for the 0.4 M DMSA condition.

The concentration of 0.3 M DMSA was chosen for all NPs coating due to characteristics obtained: small size; good PDI and; lower standard variation, that might reflect a reduced size heterogeneity.

Table 4.1. Characterization of DMSA coated SPIONs by DLS.

[DMSA] (M)	D_h[a] (nm)	PDI[b]
0.1	34.0 ± 8.6	0.39 ± 0.01
0.2	35.3 ± 3.8	0.28 ± 0.04
0.3	32.4 ± 2.1	0.34 ± 0.02
0.4	36.4 ± 3.1	0.54 ± 0.29
0.5	37.3 ± 5.1	0.28 ± 0.01

[a]D_h, hydrodynamic dyameter. [b]PDI, polydispersity index. Mean ± SD for 4 – 6 determinations is shown. For particle size, the Z-average is shown.

The SPIONs coated with DMSA were analyzed by XRD to evaluate any possible interference of the coat with the type of iron oxide species (Fig. 4.1*C*). Match software (Putz 2003) was used, as described above. The prevalent species are magnetite (65.4%) with a lower presence of maghemite (34.4%). The 2θ values for magnetite are 30.25, 35.53, 43.35, 57.14 and 62.89; and for maghemite are 30.18, 35.59, 43.28, 53.64, 57.11 and 62.79 (Appendix II).

The average grain of SPIONs coated with 0.3 M DMSA was calculated using the Scherrer's equation (Eq. 2) and the obtained size (2θ = 35.58) was 9.3 nm which indicate the size is comparable with the size obtained by DLS and also, the coating process does not promote structural changes and the surface modification might not affect the structural properties.

FTIR studies were carried out to identify of the various components present in the sample. The coupled vibrations allowed the identification of the chemical bonds of magnetite (Fe_3O_4) and DMSA. Figure 4.3 (dotted and continuous line) shows FTIR spectra of naked and DMSA coated SPIONs, respectively.

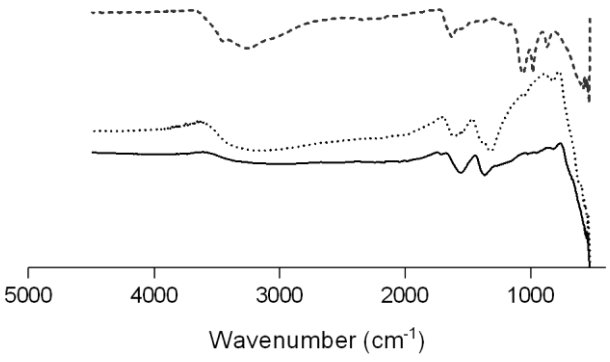

Figure 4.3. FTIR of naked SPIONs, SPIONs after surface modification with 0.3 M DMSA and functionalized SPIONs-sdAb-pepA. The dotted line corresponds to naked SPIONs, continuous line to DMSA coated SPIONs and the dashed line to SPIONs functionalized with sdAb-pepA.

From the spectra it was possible to observe the characteristic bands of magnetite at 560 cm^{-1}, the stretching vibration mode of Fe−O. At around 3200 and 1580 cm^{-1} the stretching vibration mode of −OH was observed due to the presence of water vapor (Soares *et al.* 2014). The presence of DMSA at the surface of the NPs was identified by the characteristic asymmetric and symmetric stretching of carbonyl groups at 1550 and 1310 cm^{-1}, respectively. These peaks are shifted to lower wavenumbers compared with the carbonyl absorption in free DMSA at around 1700 cm^{-1} (Palma *et al.* 2015). The absorption bands around 1090 and 930 cm^{-1} are due the vibration of C−O and $-NH_2$ of the bound proteins (peptide A and antibody) (Zhang *et al.* 2009). It is possible to conclude that the coating process and the functionalization with sdAb-pepA was successful.

The charge or electrostatic potential – zeta potential − at the surface of the nanoparticle has a significant importance in the colloidal stability of the system and can be considered an indicator of the colloidal stability due to the electrostatic interaction (Mahmoudi *et al.* 2011). NPs with values higher than +25 mV and values lower than -25 mV usually are stable, otherwise they will have a propensity to aggregate due to Van Der Wall inter-particle attraction (Mahmoudi *et al.* 2011).

Zeta potential was measured over a large pH range to determine the interval where SPIONs are stable (Table 4.2). The best zeta potential was -73.39 mV at pH 9. However, the selected pH for the functionalization procedure was 7.4 (of the PBS buffer), where the zeta-potential value is acceptable to avoid particle aggregation.

Table 4.2. The pH effect in the zeta potential of the DMSA coated SPIONs. SPIONs in solution at different pH, coated with 0.3 M DMSA.

pH	Zeta Potential (mV)
2	-4.7 ± 1.8
3	-30.0 ± 9.2
4	-47.9 ± 2.1
5	-29.5 ± 2.9
6	-33.2 ± 1.9
7	-63.1 ± 8.1
8	-67.6 ± 0.8
9	-73.4 ± 2.3
10	-58.9 ± 1.8
11	0.92 ± 0.2

Mean ± SD, for 3 – 6 determinations is shown.

Naked SPIONs have a propensity to self-associate leading to the formation of clusters, that were observed by TEM (Fig. 4.5*A*,*B*). The coat with 0.3 M DMSA provides stabilization to the NPs in solution

that decreases their tendency to form clusters (Fig.4.5*C,D*). The semispherical shape observed might be due to the type of salts that were used to produce the NPs or the ratio Fe^{2+} and Fe^{3+} (Gupta and Gupta 2005).

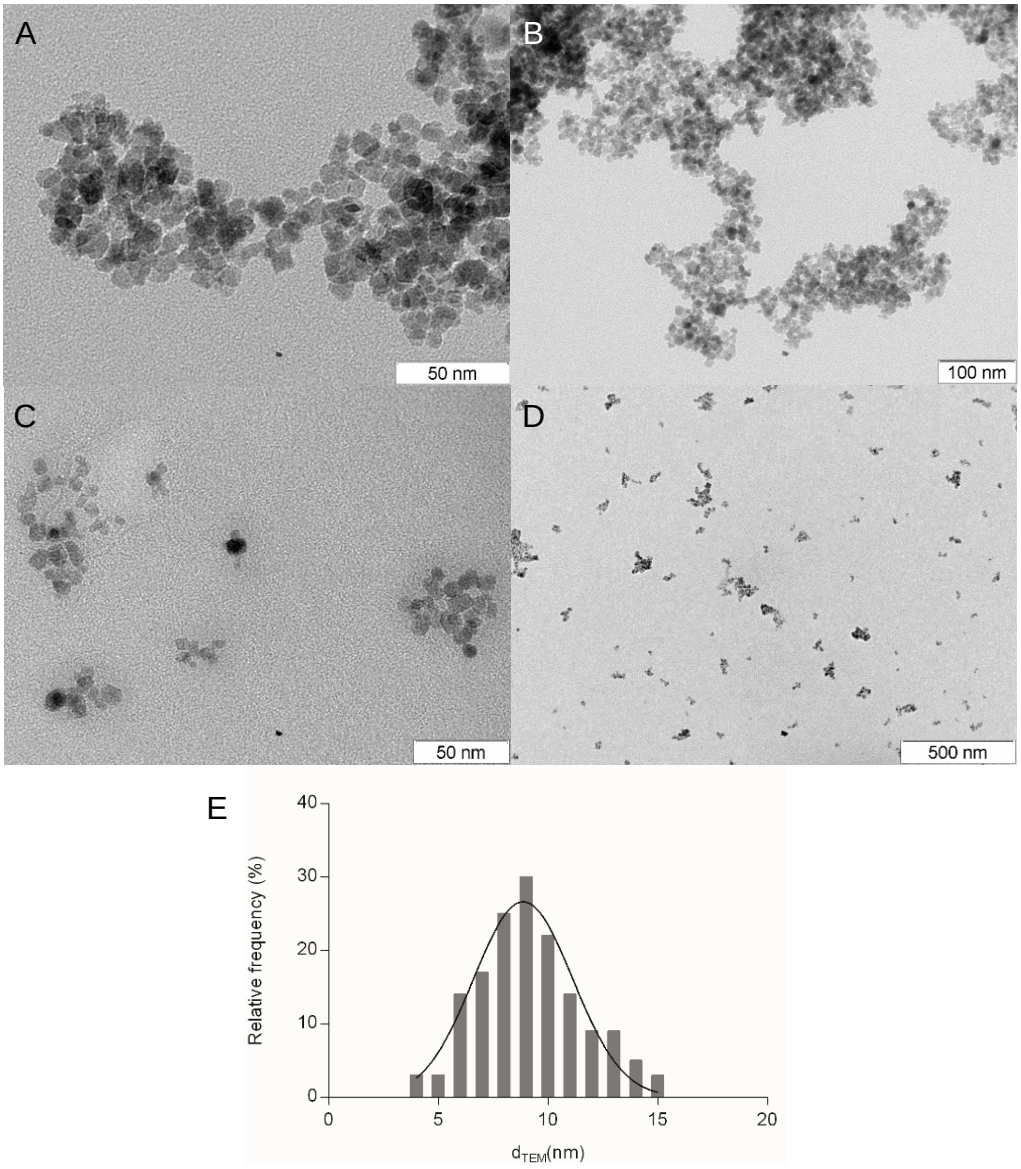

Figure 4.4. Images of SPIONs obtainded by TEM and respective size destribution. *A,B*, nacked SPIONs. *C,D*, DMSA coated SPIONs. *E*, Size distribution of DMSA coated SPIONs.

The average size of the SPIONs obtained by TEM was 9.1 ± 2.3 nm which is comparable with the size of 9.3 nm calculated with the Scherrer's equation from the XRD data.

4.3. SPIONS FUNCTIONALIZATION

SPIONs coated with 0.3 M DMSA were functionalized with three sets of proteins: GFP-pepA; sdAb and sdAB-pepA (Fig. 4.5).

Figure 4.5. sdAb-pepA sequence. The sdAb was raised against β-amyloid and pepA is a peptide derived from the dengue virus capside protein (DEN2C).

The coupling reaction is mediated by two molecules; EDC (1-ethyl-3-(3-dimethylaminopropyl) carbodiimide hydrocloride) and Sulfo-NHS (N-hydroxysulfosuccinimide) (Fig. 4.6). SPIONs have carboxylate groups on their surface created by DMSA. In the first step, EDC reacts with these carboxylate groups and creates an active-ester leaving group (*O*-acylisourea). Sulfo-NHS added in a second step, increasing the solubility and stability of the active intermediate, and promoting a better conjugation with proteins, because the sulfo-NHS ester is more reactive with the amine groups present at the surface of the proteins (N-terminal and lysine side-chain) (Scientific ; Hermanson 2013).

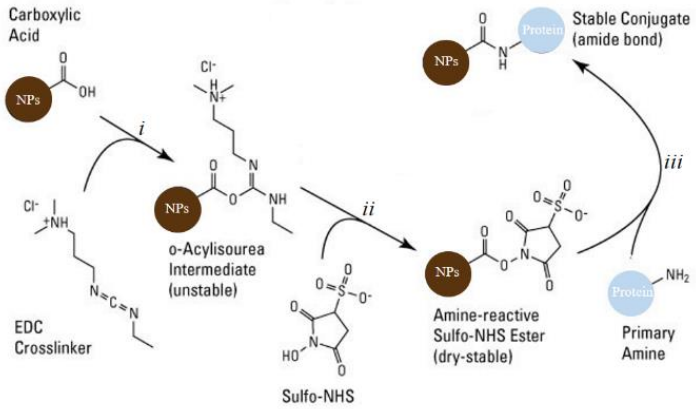

Figure 4.6. Functionalization reaction with EDC and Sulfo-NHS crosslinkers. The reaction occurs in three steps: *i*, addition of EDC to SPIONs to form a unstable o-acylisourea intermediate; *ii*, addition of sulfo-NHS forms a stable amine-reactive ester; and *iii*, reaction of the of the reactive sulfo-NHS ester with a primary amine of a protein. Adapted from (Scientific).

SPIONs were functionalized with GFP-pepA (~30 kDa) and observed by fluorescence microscopy, as a first approach to easily assess if the bio-conjugation was effective (Fig. 4.7). It was possible to observe clusters of SPIONs with GFP-pepA. The large size of the clusters might be due to the stirring process employed during coating of the NPs. This batch of SPIONs were produced using preliminary conditions, before the surface modification process with DMSA had been improved (point 4.2). A critical point during optimization of the surface modification process was the change from a mechanical stirring to an ultrasound based method during incubation with DMSA. Under mechanical stirring the dispersion could not be homogeneous, but using an ultra sounds bath during incubation of SPIONs with 0.3 M DMSA avoided this problem.

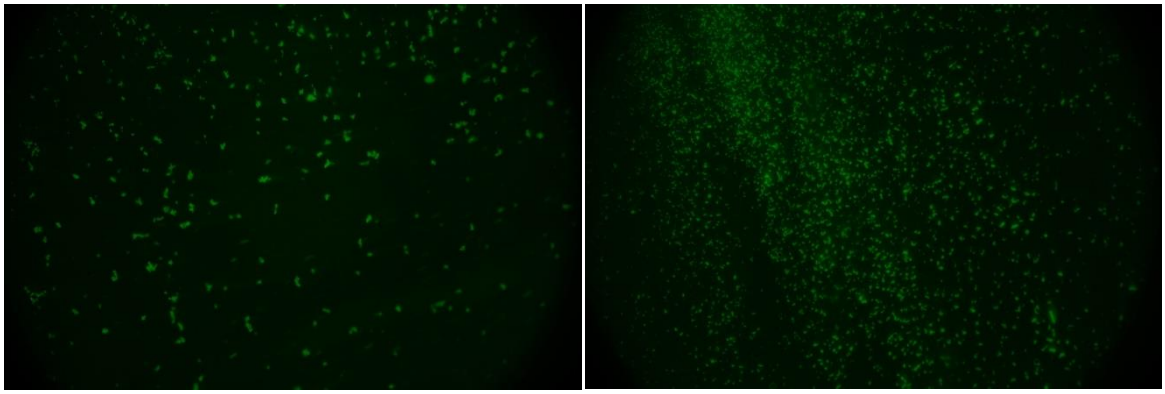

Figure 4.7. Images of SPIONs-GFP-pepA obtained by fluorescence microscopy.

After the selection of the best condition to achieve small nanoparticle size, the functionalization reaction was evaluated at two different temperatures: room temperature (~25 ºC) and 4 ºC. It was important to verify if the temperature could influence protein integrity during the 18 h of the functionalization procedure. Both conditions were analyzed by SDS-PAGE (Fig. 4.8).

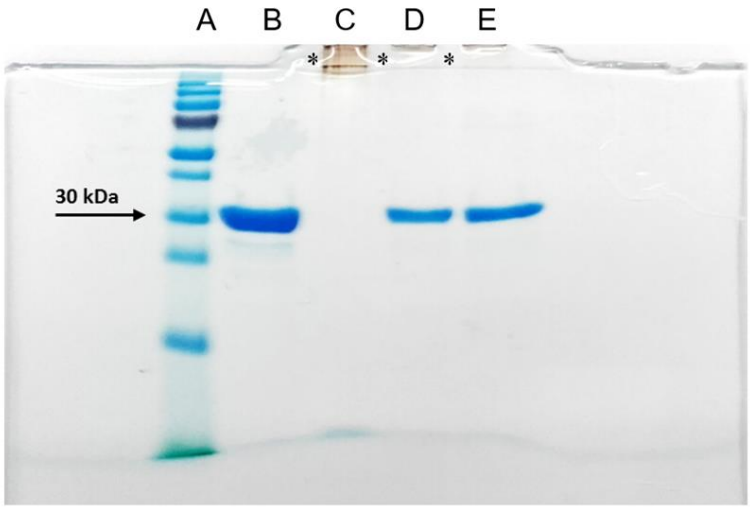

Figure 4.8. SDS-PAGE of GFP-pepA, DMSA coated SPIONs and SPIONs-GFP-pepA. *Lane A,* Protein marker; *Lane B,* GFP-pepA (10 μg); *Lane C,* DMSA coated SPIONs (6 μg, NPs); *D* and *E* SPIONs-GFP-pepA (~5 μg) after functionalization at 4ºC and RT, respectively. *SPIONs retained in the stacking gel.

The protein did not revealed proteolysis at both temperatures, although the nanoparticles at 4 ºC were less stable than at room temperature. For this reason, the selected temperature for further nanoparticle functionalization was room temperature.

4.4. CELL-BASED ASSAYS

A therapeutic delivery system to inhibit aggregation of Aβ-peptide has to be able to cross the BBB, but at the same time maintain the integrity of the BBB. A cell-based model of the BBB was used with endothelial bEnd.3 cells and a transwell apparatus to mimicking the BBB (Fig. 3.2).

4.4.1. INTEGRITY OF THE BBB MODEL

The SPIONs-GFP-pepA was incubated in the upper chamber of the transwell system and the integrity of the BBB was evaluated at different time points using a fluorescent probe FD40 that crosses the BBB when its integrity is put in risk (Fig. 4.9). After exposure to the SPIONs-GFP-pepA the integrity of the BBB decreases with longer incubation times of (Fig. 4.9*A*). However, the conjugated SPIONs seemed less harmful to the BBB than the naked SPIONs. This might be attributed to the high negative charge of the NPs, or to a more stable interaction of the BBB with the proteins at the surface of the nanoparticles in the conjugated form. An incubation time of 6 h was selected for further studies, a compromise between BBB integrity and cargo translocation across BBB.

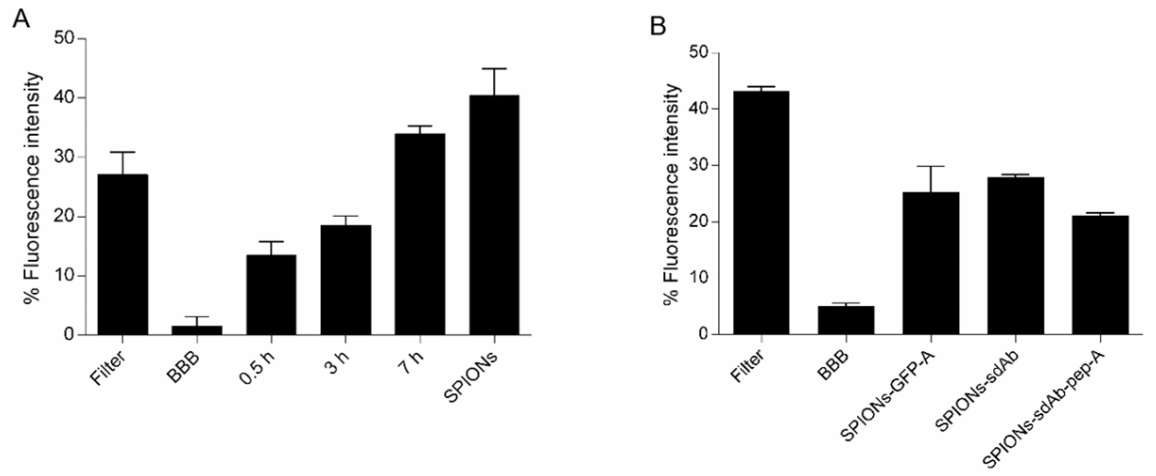

Figure 4.9. Determination of BBB integrity in the presence of conjugated SPIONs at different incubation times. *A*, SPIONs-GFP-pepA was added to the upper compartment of the BBB transwell system with bEnd.3 cells defining two compartments (upper and bottom). At defined time points the medium in the upper and bottom compartment was removed and replenishing with new medium, with the upper compartment supplemented with a fluorescent probe, FD40 (40 kDa). The fluorescence emission intensity of the probe was measured at the bottom compartment and was correlated with the integrity of the BBB. *B*, Determination of the BBB integrity in the presence of SPIONs-GFP-pepA, SPIONs-sdAb and SPIONs-sdAb-pepA at 6 h. Three controls were included: a naked transwell filter (Filter), a bEnd.3 transwell without any compound (BBB) and DMSA naked SPIONs (SPIONs). Values represent mean ± SD, n = 3.

The BBB integrity was tested with all the conjugated forms (SPIONs-GFP-pepA, SPIONs-sdAb and SPIONs-sdAb-pepA) at 6 h (Fig. 4.9*B*). The formulations affected slightly BBB integrity when compared with the BBB control, however variations in the confluence of the cells could also affect the integrity assay. Nevertheless, SPIONs-sdAb-pepA was the formulation with the lower effect in BBB integrity. Also taking in account the adverse effect of the naked SPIONs, an optimization of the ratio (SPIONs:Protein) could originate nanoparticles with no effect over BBB integrity.

4.4.2. TRANSLOCATION ACROSS THE BBB MODEL

The effectiveness of the delivery system in the transport of cargo across BBB was evaluated by the translocation assay. As a first approach, the GFP protein was used with the CPP pepA to study the translocation by using the fluorescence of GFP as an easy tool to determine the amount of protein crossing the BBB. Three time points were tested for the translocation assay (1, 3 and 6 h) (Fig.4.10*A*) and the respective BBB integrity was also assessed (Fig. 4.10*B*).

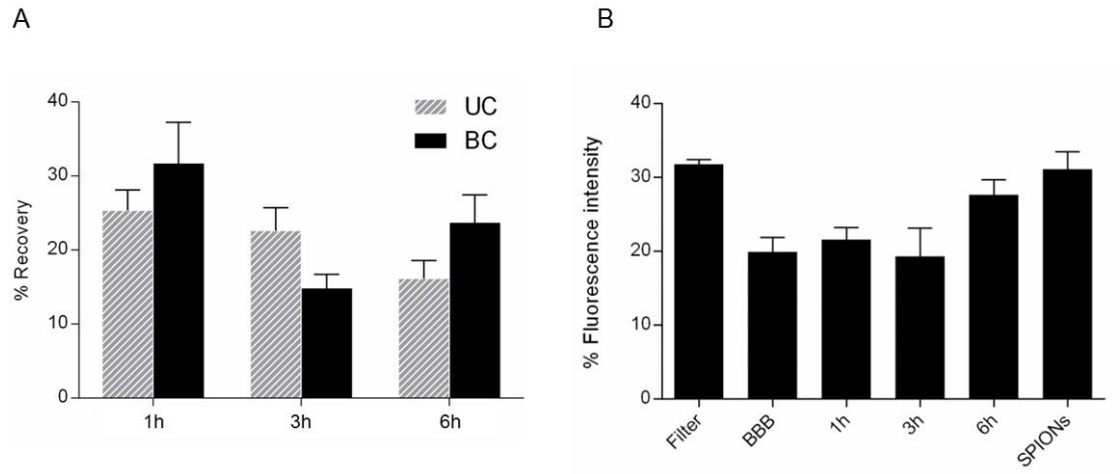

Figure 4.10. Translocation of SPIONs-GFP-pepA in the bEnd.3 transwell BB model. *A*, translocation assay of 10 μg/ml of SPIONs-GFP-pepA initially added to the upper chamber of the transwell system. After 1, 3 and 6 h incubation the relative amount of SPIONs-GFP-pepA in the upper and bottom side were quantified. The amount in the upper and bottom side was normalized to the initial total amount of SPIONs-GFP-pepA added to the top and expressed as the percentage of recovered protein. The fluorescence intensity was measured at 395 and 509 nm, considering the GFP excitation and emission wavelength, respectively. *B*, Determination of BBB integrity of SPIONs-GFP-pepA used in the translocation assay. The fluorescence emission intensity of the probe FD40 was measured at the bottom compartment and was correlated with the integrity of the BBB. Values represent mean ± SD, n = 3.

The amount of functionalized SPIONs-GFP-pepA decreased in the upper chamber during the time course of the assay and increased in the bottom chamber. However, at 1 h the recovery at the bottom chamber is very high and do not match the trend at the other time points. The integrity of the BBB in the presence of the SPIONs-GFP-pepA was higher with lower incubation times. However, the BBB control for the integrity was similar to 1 and 3 h incubation, what may indicate that the cells confluence was not optimal. The recovered value of the protein was not the total amount introduced in the upper chamber. This led us to evaluate if the formulation was interacting with the membrane of the cells or was internalized in the cells by performing an uptake assay (Appendix III). The results were inconclusive because the amount of the NPs could not be traced in all conditions.

The translocation of SPIONs-sdAb-pepA was followed by Western blot using an antibody anti-His tag present in the protein. The SPIONs-GFP-pepA was also used in the translocation assay and Western blot detection as a positive control, because its translocation was already known to occur from previous assays (Fig. 4.10 and Fig. 4.11*A*, *inset*).

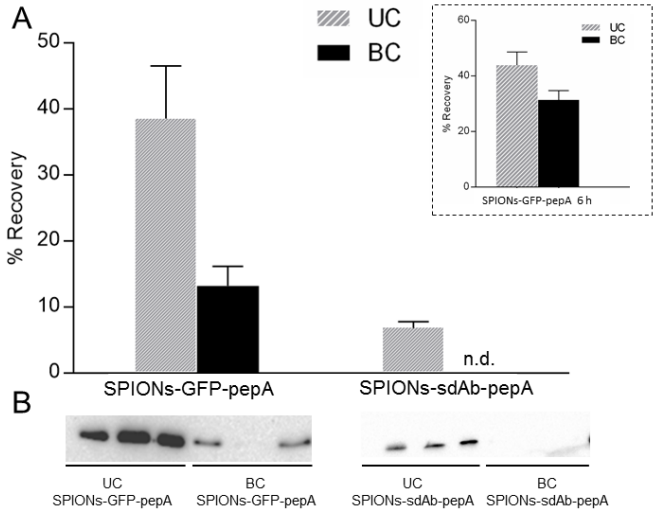

Figure 4.11. Translocation of SPIONs-GFP-pepA and SPIONs-sdAb-pepA in the bEnd.3 transwell BBB evaluated by western blot. *A*, Translocation assay of 10 μg/ml of SPIONs-GFP-pepA or SPIONs-sdAb-pepA initially added to the upper chamber of the transwell system. The detection of SPIONs-GFP-pepA of this formulation batch was also tested by fluorescence detection (*inset*). *B*, after 6 h incubation the relative amount of protein in the upper and bottom sides was quantified by Western blot. For immunodetection, a conjugate anti-His-HRP mAb was used. As positive control of the anti-His-HRP detection, 100 ng of purified GFP-pepA or sdAb-pepA was used. The (%) of recovery was determined as the ratio of the protein detected in each chamber after 6 h to the total amount of protein added to the upper chamber at the beginning of the assay. n.d., not detected.

The translocation of the SPIONs-GFP-pepA was also confirmed by Western blot detection (Fig. 4.11*A*). The recovered values obtained by fluorescence detection and Western blot were 31.4 ± 3.3 and 13.2 ± 2.9 %, respectively.

In the translocation assay of SPIONs-sdAb-pepA no protein was detected in the bottom chamber and only a small fraction was detected in the upper chamber. One possibility for this difference is the fact that the fusion protein of sdAb-pepA could affect the cell penetrating function of pepA. If this turns out to be the case, a different N-terminal fusion maybe be evaluated (SPIONs-pepA-sdAb). Other possibility is the internalization of the SPIONs-sdAb-pepA and hence the cellular uptake of this formulation should be evaluated, as well as the type of interaction of the SPIONs-sdAb-pepA with the cell membrane (receptor mediator transcytosis – RMT versus adsorptive mediated transcytosis – AMT) (Jones and Shusta 2007).

4.4.3. INHIBITION OF β-AMYLOID AGGREGATION BY CONJUGATED SPIONS

The sdAb used in this study it able to inhibit β-amyloid aggregation (Lauwereys *et al.* 2008). The antibody or the antibody peptide–A were conjugated to the iron oxide NPs via the primary amines of the protein. In order to test if the antibody retained the ability to inhibit β-amyloid aggregation, when fused to pepA and/or bound to the SPIONs, a Thioflavin-T (ThT) based assay was performed (Fig. 4.12).

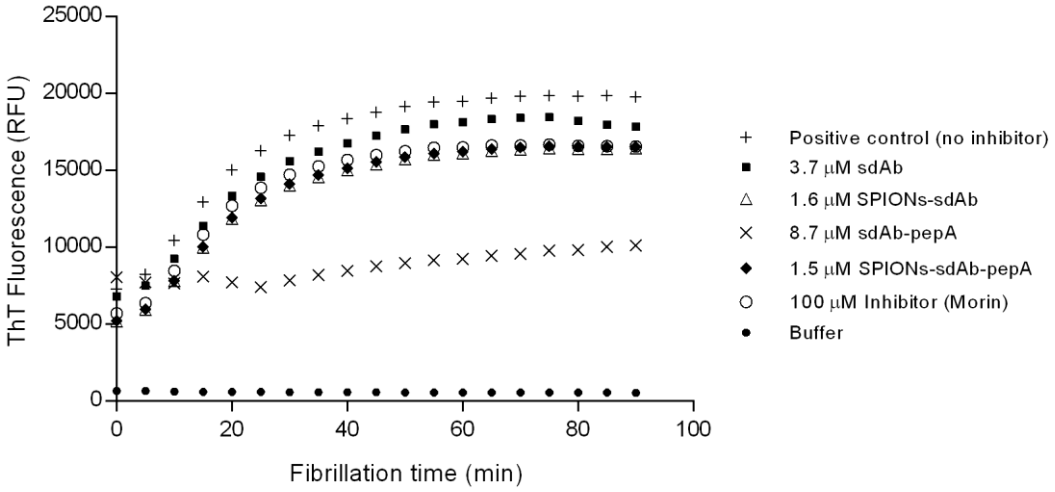

Figure 4.12. Inhibition assay. Fibrillation kinetic curves determined by thioflavin T assay for amyloid-β42 peptide (46 μM) in the absence (+, positive control) and presence of unconjugated sdAb (■) and sdAb-pepA(×), and conjugate versions: SPIONs–sdAb (Δ) and SPIONs–sdAb-pepA (♦) at different concentrations. Morin, a known inhibitor of amyloid-β42 aggregation was used as control (○) and a buffer control was included (●). The fluorescence intensity was measured at 37 ºC using an excitation of 440 nm and emission of 484 nm. The SensoLyte Thioflavin T β-Amyloid (1-42) Aggregation Kit (AnaSpec) was used.

The β-amyloid (1-42) (Aβ42) peptide starts to aggregate after a lag phase of ~5min and reaches a plateau of ~20,000 RFU for the tested concentration of Aβ42 (46 μM). Morin, a known inhibitor of Aβ42, aggregation was used at 100 μM final concentration and it was able to reduce the extent of aggregation to ~16,000 RFU (16% inhibition). The unconjugated antibody (sdAb and sdAb-pepA) and the conjugated forms (SPIONs-sdAb and SPIONs-sdAb-pepA) were initially intended to be tested at the same concentration. However, the conjugated SPIONs batch had a lower concentration of the protein thus preventing the use of the same concentration in all samples (a higher concentration of the unconjugated samples was used to see the inhibition effect of the antibody).

The SPIONs-sdAb was able to inhibit (17%) slightly better the aggregation of Aβ42, even compared with a higher concentration of the unconjugated sdAb (7% of inhibition). When comparing the two conjugated forms (SPIONs-sdAb and SPIONs-sdAb-pepA) it is possible to observe that the cell penetrating peptide A does not affect the action of the antibody (17% for both). The sdAb-pepA revealed

the highest inhibition of Aβ42 aggregation (52%), however this form was tested at a higher concentration.

The two nanoparticles formulations (SPIONs-sdAb and SPIONs-sdAb-pepA) were tested at a low concentration but exhibited a similar inhibition level (17%) when compared with the inhibitor morin (16%). Therefor the conjugation of the antibody to the nanoparticles does not appear to affect its function.

Part V

Concluding Remarks and Future Perspectives

Central nervous system (CNS) disorders affect up to 1 billion people worldwide. It is estimated that Alzheimer and other dementias constitute 3% of the total deaths in 2015. The number is expected to double every 20 years. There is a lack of therapies to treat these disorders due to the properties of blood brain barrier (BBB). The BBB restricts the transfer of therapeutic molecules between the blood and the brain. Therefore, there is a need to find molecules that can overcome this obstacle and carry with them the drugs. These can either be achieved through targeting of brain receptors, via receptor-mediated transport (RMT); or through adsorptive-mediated transcytosis (AMT). Cell penetrating peptides (CPP) have been investigated has a drug delivery system due to their ability to cross cell membrane, and are expected to also be able to transport different cargos across the BBB.

Alzheimer's disease is characterized by an accumulation of amyloid–β (Aβ) aggregates in the brain. Antibodies that recognize Aβ can be used not only for targeted imaging but also as promising immunotherapy for AD, by stopping Aβ aggregation.

There is an urgent need to detect AD in early stages, avoiding the decline of the brain functions and cell death. Usually, the disease is detected using imaging techniques (magnetic resonance of imaging (MRI) or positron emission tomography), that only allow to detect later stages of the disease.

The possibility to develop a theranostic system that combines the early diagnostic and the therapy might be a progress for the treatment of AD.

The main goal of this project was to develop a drug delivery system able to cross the blood brain barrier (BBB) with therapeutic properties to tackle Alzheimer's disease. The system comprises superparamagnetic iron oxide nanoparticles (SPIONs), a cell penetrating peptide (pepA) and an antibody against β-amyloid (sdAb).

Initially, iron oxide nanoparticles were synthetized by chemical co-precipitation method with subsequent oxidation. The main purpose of the oxidation was to obtain maghemite species (γ-Fe_2O_3), a more stable specie. The oxidation of the SPIONs was evaluated in two different conditions: temperature (condition I) and pH (condition II). For both conditions a mixture of maghemite and magnetite was present. The oxidation condition through pH was the one selected for three main reasons *i*) SPIONs were more stable by pH oxidation; *ii*) after characterization it was possible to conclude that the size of the nanoparticles was similar between both conditions (8 and 8.9 nm for condition I and II, respectively) and *iii*) the subsequent NPs surface modification reaction had to proceed at pH 3.

The SPIONs surface modification with DMSA was tested at different concentrations. The 0.3 M DMSA condition was selected due to lower size of the NPs obtained, determined by DLS. The properties of the iron oxide nanoparticles were analyzed after modification and no alteration of properties was observed with coating (size, crystalline structure). In addition, the coating consefered further stability to the nanoparticles.

Furhter functionalization of DMSA coated SPIONS with GFP-pepA, sdAb and sdAb-pepA was successful achieved. Reactions at either at 4 ºC or room temperature, resulted in conservation of protein integrity as analyzed by SDS-PAGE.

The drug delivery system was tested in endothelial cells (bEnd.3) using a transwell system to mimicking the BBB. The integrity of the cells and the translocation were evaluated. SPIONs and SPIONs-GFP-pepA had some effect on the BBB integrity, but SPIONs-sdAb-pepA was the formulation with lower impact on the endothelial cell barrier (SPIONs-sdAb-pepA < SPIONs-GFP-pepA < SPIONs). After 6 h, 23.7 ± 3.7 % of SPIONs-GFP-pepA successfully crossed the BBB, but the same was not observed for SPIONs-sdAb-pepA. Further studies need to be carried out to understand this behavior, but a possible explanation might be related to protein rearrangement during functionalization and consequent blocking of pepA properties to cross the BBB.

sdAb, sdAb-pepA, SPIONs-sdAb and SPIONs-sdAb-pepA were able to inhibit the aggregation of β-amyloid protein, when compared with a Morin (commercially available inhibitor). The functionalization of the SPIONs with the antibody does not seem to affect function of the latter. Moreover, SPIONs-sdAb is able to inhibit β-amyloid aggregation at a lower concentration where compared with sdAb alone.

In general, the theranostic drug delivery system was successfully developed, but further optimization will be necessary. SPIONs-sdAb-pepA formulations have to be modified due to the lack translocation across the BBB. The order of the proteins in the fusion protein can be reversed with the CPP at the N-terminal (SPIONs-pepA-sdAb), or different size linkers between the two proteins can be evaluated (SPIONs-sdAb-$(linker)_n$-pepA), in order to maintain the cell penetration ability of the peptide.

The ratio of SPIONs:protein should also be studied during the functionalization and optimized. Naked SPIONs affected the integrity of the BBB, but the effect decreased with functionalization. A lower ratio of SPIONs:protein might decrease even further the adverse effect on the integrity of the BBB.

The system has also to be tested by magnetic resonance imaging to evaluate the full potential of the system.

In conclusion, the system is able to play their dual function: the diagnostic (using the SPIONs as a contrast agent) and the therapy, (using the sdAb to bind the Aβ peptides). Although, this system has other advantage: the pepA, allows it to cross the BBB and get to the target in the brain, to exert its function.

Application of this drug delivery system to other CNS diseases might be discovered in the future, for instance, through the replacement of sdAb by other antibody that recognize the protein aggregates related to Parkinson disease.

References

Albert M., DeCarli C., DeKosky S., Leon M., Foster N. L., Fox N., Frank R., Frackowiak R., Jack C., Jagust W. J., Knopman D., Morris J. C., Petersen R. C., Reiman E., Scheltens P., Small G., Soininen H., Thal L., Wahlund L., Thies W., Weiner M. W. and Khachaturian Z., The Use of MRI and PET for Clinical Diagnosis of Dementia and Investigation of Cognitive Impairment: A Consensus Report, in: Alzheimer's Association Neuroimaging Work Group Consensus Report.

Andrieux K. and Couvreur P. (2013) Nanomedicine as a promising approach for the treatment and diagnosis of brain diseases: the example of Alzheimer's disease. *Ann. Pharm. Fr.* 71: 225-233.

Banks W. A. and Erickson M. A. (2010) The blood-brain barrier and immune function and dysfunction. *Neurobiol. Dis.* 37: 26-32.

Biancalana M. and Koide S. (2010) Molecular mechanism of Thioflavin-T binding to amyloid fibrils. *Biochim. Biophys. Acta* 1804: 1405-1412.

Bradford M. M. (1976) A rapid and sensitive method for the quantitation of microgram quantities of protein utilizing the principle of protein-dye binding. *Anal. Biochem.* 72: 248-254.

Brown R. C., Morris A. P. and O'Neil R. G. (2007) Tight junction protein expression and barrier properties of immortalized mouse brain microvessel endothelial cells. *Brain Res.* 1130: 17-30.

Busquets M. A., Sabate R. and Estelrich J. (2014) Potential applications of magnetic particles to detect and treat Alzheimer's disease. *Nanoscale Res Lett* 9: 538.

Calero M., Gutierrez L., Salas G., Luengo Y., Lazaro A., Acedo P., Morales M. P., Miranda R. and Villanueva A. (2014) Efficient and safe internalization of magnetic iron oxide nanoparticles: two fundamental requirements for biomedical applications. *Nanomedicine* 10: 733-743.

Castanho M. A., Neves V. and Aires da Silva F., Design of Peptides for brain delivery, in, vol. IMM INPI20151000007982, 2015.

Cecchelli R., Berezowski V., Lundquist S., Culot M., Renftel M., Dehouck M. P. and Fenart L. (2007) Modelling of the blood-brain barrier in drug discovery and development. *Nat Rev Drug Discov* 6: 650-661.

Corte-Real S., Neves V., Canhão P., Outeiro T., Castanheira N. and Santiago S., Antibody molecules and peptide delivery systems for use in Alzheimer's disease and related disorders, in, Portugal, 2016.

Costa D. M., Grave E., Bakker P. M. A. and Vandenberghe V. E. (1994) Synthesis and Characterization of Some Iron Oxides by Sol-Gel Method. *J. Solid State Chem.* 113: 405-412.

Cummings J. L., Morstorf T. and Zhong K. (2014) Alzheimer's disease drug-development pipeline: few candidates, frequent failures. *Alzheimers Res. Ther.* 6: 37.

Daneschvar H. L., Aronson M. D. and Smetana G. W. (2015) Do statins prevent Alzheimer's disease? A narrative review. *Eur. J. Intern. Med.*

de Boer A. G. and Gaillard P. J. (2007) Drug targeting to the brain. *Annu. Rev. Pharmacol. Toxicol.* 47: 323-355.

Deguchi Y. (2002) Application of in vivo brain microdialysis to the study of blood-brain barrier transport of drugs. *Drug Metab. Pharmacokinet.* 17: 395-407.

Eiriksdottir E., Konate K., Langel U., Divita G. and Deshayes S. (2010) Secondary structure of cell-penetrating peptides controls membrane interaction and insertion. *Biochim. Biophys. Acta* 1798: 1119-1128.

Faiyas A. P. A., Vinod E. M., Joseph J., Ganesan R. and Pandey R. K. (2010) Dependence of pH and surfactant effect in the synthesis of magnetite (Fe3O4) nanoparticles and its properties. *J. Magn. Magn. Mater.* 322: 400-404.

Fauconnier N., Pons J. N., Roger J. and Bee A. (1997) Thiolation of Maghemite Nanoparticles by Dimercaptosuccinic Acid. *J. Colloid Interface Sci.* 194: 427-433.

Freire J. M., Veiga A. S., Conceicao T. M., Kowalczyk W., Mohana-Borges R., Andreu D., Santos N. C., Da Poian A. T. and Castanho M. A. (2013) Intracellular nucleic acid delivery by the supercharged dengue virus capsid protein. *PLoS One* 8: e81450.

Freire J. M., Veiga A. S., Rego de Figueiredo I., de la Torre B. G., Santos N. C., Andreu D., Da Poian A. T. and Castanho M. A. (2014) Nucleic acid delivery by cell penetrating peptides derived from dengue virus capsid protein: design and mechanism of action. *FEBS J* 281: 191-215.

Frisoni G. B., Fox N. C., Jack C. R., Scheltens P. and Thompson P. M. (2010) The clinical use of structural MRI in Alzheimer disease. *Nature Reviews Neurology* 6: 67-77.

Garcia M. P., Parca R. M., Chavesa S. M., Silva L. P., Santosa A. D., Lacava Z. G., Morais P. C. and Azevedo R. B. (2005) Morphological analysis of mouse lungs after treatment with magnetite-based magnetic fluid stabilized with DMSA. *J. Magn. Magn. Mater.* 293 277-282.

Ge G., Wu H., Xiong F., Zhang Y., Guo Z., Bian Z., Xu J., Gu C., Gu N., Chen X. and Yang D. (2013) The cytotoxicity evaluation of magnetic iron oxide nanoparticles on human aortic endothelial cells. *Nanoscale Res Lett* 8: 215.

Giacobini E. and Gold G. (2013) Alzheimer disease therapy--moving from amyloid-beta to tau. *Nat. Rev. Neurol.* 9: 677-686.

Gnanaprakash G., Mahadevan S., Jayakumar T., Kalyanasundaram P., Philip J. and Raj B. (2007) Effect of initial pH and temperature of iron salt solutions on formation of magnetite nanoparticles. *Mater. Chem. Phys.* 103: 168-175.

Goldburg W. I. (1999) Dynamic light scattering. *American Association of Physics Teachers* 67: 1152-1160.

Gupta A. K. and Gupta M. (2005) Synthesis and surface engineering of iron oxide nanoparticles for biomedical applications. *Biomaterials* 26: 3995-4021.

Hadj Farhat M. A. and Joubert J. C. (1984) Hydrothermal synthesis and characterisation of the hexagonal ferrite Fe2-Y. *J. Magn. Magn. Mater.* 62: 353-358.

Hames B. D., Gel electrophoresis of proteins : a practical approach, 3rd ed., Oxford University Press, Oxford ; New York, 1998.

Helms H. C., Hersom M., Kuhlmann L. B., Badolo L., Nielsen C. U. and Brodin B. (2014) An electrically tight in vitro blood-brain barrier model displays net brain-to-blood efflux of substrates for the ABC transporters, P-gp, Bcrp and Mrp-1. *AAPS J* 16: 1046-1055.

Heppner F. L., Ransohoff R. M. and Becher B. (2015) Immune attack: the role of inflammation in Alzheimer disease. *Nat. Rev. Neurosci.* 16: 358-372.

Herholz K., Carter S. F. and Jones M. (2007) Positron emission tomography imaging in dementia. *Br. J. Radiol.* 80 Spec No 2: S160-167.

Hermanson G. T., Bioconjugate Techniques, Third edition ed., Elsevier, London, 2013.

Hola K., Markova Z., Zoppellaro G., Tucek J. and Zboril R. (2015) Tailored functionalization of iron oxide nanoparticles for MRI, drug delivery, magnetic separation and immobilization of biosubstances. *Biotechnol Adv* 33: 1162-1176.

Holmes C., Wilkinson D., Dean C., Vethanayagam S., Olivieri S., Langley A., Pandita-Gunawardena N. D., Hogg F., Clare C. and Damms J. (2004) The efficacy of donepezil in the treatment of neuropsychiatric symptoms in Alzheimer disease. *Neurology* 63: 214-219.

Jafari S., Maleki Dizaj S. and Adibkia K. (2015) Cell-penetrating peptides and their analogues as novel nanocarriers for drug delivery. *Bioimpacts* 5: 103-111.

Johnson K. A., Fox N. C., Sperling R. A. and Klunk W. E. (2012) Brain imaging in Alzheimer disease. *Cold Spring Harb. Perspect. Med.* 2: a006213.

Jones A. R. and Shusta E. V. (2007) Blood-brain barrier transport of therapeutics via receptor-mediation. *Pharm. Res.* 24: 1759-1771.

Khurana R., Coleman C., Ionescu-Zanetti C., Carter S. A., Krishna V., Grover R. K., Roy R. and Singh S. (2005) Mechanism of thioflavin T binding to amyloid fibrils. *J. Struct. Biol.* 151: 229-238.

Kim D. K., Zhang Y., Voit W., Rao K. V. and Muhammed M. (2001) Synthesis and characterization of surfactant-coated superparamagnetic monodispersed iron oxide nanoparticles. *J. Magn. Magn. Mater.* 225: 30-36.

Kristensen M., Birch D. and Morck Nielsen H. (2016) Applications and Challenges for Use of Cell-Penetrating Peptides as Delivery Vectors for Peptide and Protein Cargos. *Int J Mol Sci* 17.

Kummer M. P. and Heneka M. T. (2014) Truncated and modified amyloid-beta species. *Alzheimers Res. Ther.* 6: 28.

Laurent S., Forge D., Port M., Roch A., Robic C., Vander Elst L. and Muller R. N. (2008) Magnetic iron oxide nanoparticles: synthesis, stabilization, vectorization, physicochemical characterizations, and biological applications. *Chem. Rev.* 108: 2064-2110.

Lauwereys M., Van Leuven F., Van Der Auwera I., Wera S. and Merchiers P., Nanobodies Tm Against Amyloid-Beta and Polypeptides Comprising the Same for the Treatment of Degenerative Neural Diseases Such as Alzheimer's Disease, in, Google Patents, 2008.

Lee N. and Hyeon T. (2012) Designed synthesis of uniformly sized iron oxide nanoparticles for efficient magnetic resonance imaging contrast agents. *Chem. Soc. Rev.* 41: 2575-2589.

Li L., Jiang W., Luo K., Song H., Lan F., Wu Y. and Gu Z. (2013) Superparamagnetic iron oxide nanoparticles as MRI contrast agents for non-invasive stem cell labeling and tracking. *Theranostics* 3: 595-615.

Lim E. K., Jang E., Lee K., Haam S. and Huh Y. M. (2013a) Delivery of cancer therapeutics using nanotechnology. *Pharmaceutics* 5: 294-317.

Lim J., Yeap S. P., Che H. X. and Low S. C. (2013b) Characterization of magnetic nanoparticle by dynamic light scattering. *Nanoscale Res Lett* 8: 381.

Lindberg D. J., Wranne M. S., Gilbert Gatty M., Westerlund F. and Esbjorner E. K. (2015) Steady-state and time-resolved Thioflavin-T fluorescence can report on morphological differences in amyloid fibrils formed by Abeta(1-40) and Abeta(1-42). *Biochem. Biophys. Res. Commun.* 458: 418-423.

Ling D. and Hyeon T. (2013) Chemical design of biocompatible iron oxide nanoparticles for medical applications. *Small* 9: 1450-1466.

Liu J., Yang B., Ke J., Li W. and Suen W. C. (2016) Antibody-Based Drugs and Approaches Against Amyloid-beta Species for Alzheimer's Disease Immunotherapy. *Drugs Aging*.

López-Pérez J. A., López-Quintela M. A., Mira J., Rivas J. and Charles S. W. (1997) Advances in the Preparation of Magnetic Nanoparticles by the Microemulsion Method. *The journal of physical chemistry B* 101.

Lu J. X., Qiang W., Yau W. M., Schwieters C. D., Meredith S. C. and Tycko R. (2013) Molecular structure of beta-amyloid fibrils in Alzheimer's disease brain tissue. *Cell* 154: 1257-1268.

Madani F., Lindberg S., Langel U., Futaki S. and Graslund A. (2011) Mechanisms of cellular uptake of cell-penetrating peptides. *J Biophys* 2011: 414729.

Mahmoudi M., Sant S., Wang B., Laurent S. and Sen T. (2011) Superparamagnetic iron oxide nanoparticles (SPIONs): development, surface modification and applications in chemotherapy. *Adv Drug Deliv Rev* 63: 24-46.

Mairuhu A. T., Wagenaar J., Brandjes D. P. and van Gorp E. C. (2004) Dengue: an arthropod-borne disease of global importance. *Eur. J. Clin. Microbiol. Infect. Dis.* 23: 425-433.

Malvern, Zetasizer Nano User Manual, Malvern, Worcestershire, 2013.

Martin L., Latypova X., Wilson C. M., Magnaudeix A., Perrin M. L., Yardin C. and Terro F. (2013) Tau protein kinases: involvement in Alzheimer's disease. *Ageing Res Rev* 12: 289-309.

Massart R., Magnetic fluids and process for obtaining them, in: Agence Nationale de Valorisation de la Recherche (ANVAR) (Ed.), France, 1980.

Matharu B., Spencer N., Howe F. and Austen B. (2015) Gadolinium-complexed Abeta-binding contrast agents for MRI diagnosis of Alzheimer's Disease. *Neuropeptides* 53: 63-70.

Maurer K., Volk S. and Gerbaldo H. (1997) Auguste D and Alzheimer's disease. *Lancet* 349: 1546-1549.

Mejias R., Perez-Yague S., Roca A. G., Perez N., Villanueva A., Canete M., Manes S., Ruiz-Cabello J., Benito M., Labarta A., Batlle X., Veintemillas-Verdaguer S., Morales M. P., Barber D. F. and Serna C. J. (2010) Liver and brain imaging through dimercaptosuccinic acid-coated iron oxide nanoparticles. *Nanomedicine (Lond)* 5: 397-408.

Mejias R., Perez-Yague S., Gutierrez L., Cabrera L. I., Spada R., Acedo P., Serna C. J., Lazaro F. J., Villanueva A., Morales Mdel P. and Barber D. F. (2011) Dimercaptosuccinic acid-coated magnetite nanoparticles for magnetically guided in vivo delivery of interferon gamma for cancer immunotherapy. *Biomaterials* 32: 2938-2952.

Mendiola-Precoma J., Berumen L. C., Padilla K. and Garcia-Alcocer G. (2016) Therapies for Prevention and Treatment of Alzheimer's Disease. *Biomed Res Int* 2016: 2589276.

Meyer-Luehmann M., Coomaraswamy J., Bolmont T., Kaeser S., Schaefer C., Kilger E., Neuenschwander A., Abramowski D., Frey P., Jaton A. L., Vigouret J. M., Paganetti P., Walsh D. M., Mathews P. M., Ghiso J., Staufenbiel M., Walker L. C. and Jucker M. (2006) Exogenous induction of cerebral beta-amyloidogenesis is governed by agent and host. *Science* 313: 1781-1784.

Murphy M. P. and LeVine H., 3rd (2010) Alzheimer's disease and the amyloid-beta peptide. *J. Alzheimers Dis.* 19: 311-323.

Muruganandam A., Tanha J., Narang S. and Stanimirovic D. (2002) Selection of phage-displayed llama single-domain antibodies that transmigrate across human blood-brain barrier endothelium. *FASEB J.* 16: 240-242.

Nakagawa S., Deli M. A., Kawaguchi H., Shimizudani T., Shimono T., Kittel A., Tanaka K. and Niwa M. (2009) A new blood-brain barrier model using primary rat brain endothelial cells, pericytes and astrocytes. *Neurochem. Int.* 54: 253-263.

Neves V., Aires-da-Silva F., Corte-Real S. and Castanho M. A. R. B. (2016) Antibody Approaches To Treat Brain Diseases. *Trends Biotechnol.* 34.

Niewoehner J., Bohrmann B., Collin L., Urich E., Sade H., Maier P., Rueger P., Stracke J. O., Lau W., Tissot A. C., Loetscher H., Ghosh A. and Freskgard P. O. (2014) Increased brain penetration and potency of a therapeutic antibody using a monovalent molecular shuttle. *Neuron* 81: 49-60.

Nordberg A. (2015) Dementia in 2014. Towards early diagnosis in Alzheimer disease. *Nat. Rev. Neurol.* 11: 69-70.

Obermeier B., Daneman R. and Ransohoff R. M. (2013) Development, maintenance and disruption of the blood-brain barrier. *Nat. Med.* 19: 1584-1596.

Palma S. I., Marciello M., Carvalho A., Veintemillas-Verdaguer S., Morales Mdel P. and Roque A. C. (2015) Effects of phase transfer ligands on monodisperse iron oxide magnetic nanoparticles. *J. Colloid Interface Sci.* 437: 147-155.

Pardridge W. M. (2005) The blood-brain barrier: bottleneck in brain drug development. *NeuroRx* 2: 3-14.

Pérez M. J., Jara C., Muñoz-Urrutia E. and Quintanilla R. A., New Targets for Diagnosis and Treatment Against Alzheimer's Disease: The Mitochondrial Approach, in, 2016.

Prades R., Oller-Salvia B., Schwarzmaier S. M., Selva J., Moros M., Balbi M., Grazu V., de La Fuente J. M., Egea G., Plesnila N., Teixido M. and Giralt E. (2015) Applying the retro-enantio approach to obtain a peptide capable of overcoming the blood-brain barrier. *Angew. Chem. Int. Ed. Engl.* 54: 3967-3972.

Putz H., MATCH! Pahse identification from Powder Diffraction, in, Germany, 2003.

Rebodos R. L. and Vikesland P. J. (2010) Effects of oxidation on the magnetization of nanoparticulate magnetite. *Langmuir* 26: 16745-16753.

Reiman E. M. (2016) Alzheimer's disease: Attack on amyloid-beta protein. *Nature* 537: 36-37.

Reitz C. (2012) Alzheimer's disease and the amyloid cascade hypothesis: a critical review. *Int. J. Alzheimers Dis.* 2012: 369808.

Risacher S. L. and Saykin A. J. (2013) Neuroimaging and other biomarkers for Alzheimer's disease: the changing landscape of early detection. *Annu. Rev. Clin. Psychol.* 9: 621-648.

Ruiz A., Morais P. C., Azevedo R. B., Lacava Z. G. M., Villanueva A. and Morale M. P. (2014) Magnetic nanoparticles coated with dimercaptosuccinic acid: development, characterization, and application in biomedicine. *J Nanopart Res* 16: 2589.

Rümenapp C., Gleich B. and Haase A. (2012) Magnetic Nanoparticles in Magnetic Resonance Imaging and Diagnostics. *Pharm. Res.* 29: 1165-1179.

Ryu J. H., Lee S., Son S., Kim S. H., Leary J. F., Choi K. and Kwon I. C. (2014) Theranostic nanoparticles for future personalized medicine. *J. Control. Release* 190: 477-484.

Sala Frigerio C. and De Strooper B. (2016) Alzheimer's Disease Mechanisms and Emerging Roads to Novel Therapeutics. *Annu. Rev. Neurosci.* 39: 57-79.

Santhosh P. B. and Ulrih N. P. (2013) Multifunctional superparamagnetic iron oxide nanoparticles: promising tools in cancer theranostics. *Cancer Lett.* 336: 8-17.

Santos S., Torcato I. and Castanho M. A. (2012) Biomedical applications of dipeptides and tripeptides. *Biopolymers* 98: 288-293.

Sarko D., Beijer B., Garcia Boy R., Nothelfer E. M., Leotta K., Eisenhut M., Altmann A., Haberkorn U. and Mier W. (2010) The pharmacokinetics of cell-penetrating peptides. *Mol. Pharm.* 7: 2224-2231.

Scientific T. F. "Carbodiimide Crosslinker Chemistry." Retrieved October, 10, 2016, from https://www.thermofisher.com/us/en/home/life-science/protein-biology/protein-biology-learning-center/protein-biology-resource-library/pierce-protein-methods/carbodiimide-crosslinker-chemistry.html.

Sevigny J., Chiao P., Bussiere T., Weinreb P. H., Williams L., Maier M., Dunstan R., Salloway S., Chen T., Ling Y., O'Gorman J., Qian F., Arastu M., Li M., Chollate S., Brennan M. S., Quintero-Monzon O., Scannevin R. H., Arnold H. M., Engber T., Rhodes K., Ferrero J., Hang Y., Mikulskis A., Grimm J., Hock C., Nitsch R. M. and Sandrock A. (2016) The antibody aducanumab reduces Abeta plaques in Alzheimer's disease. *Nature* 537: 50-56.

Shevtsov M. A., Nikolaev B. P., Ryzhov V. A., Yakovleva L. Y., Dobrodumov A. V., Marchenko Y. Y., Margulis B. A., Pitkin E. and Guzhova I. V. (2015) Brain tumor magnetic targeting and biodistribution of superparamagnetic iron oxide nanoparticles linked with 70-kDa heat shock protein study by nonlinear longitudinal response. *J. Magn. Magn. Mater.* 388: 123-134.

Sisodia S. S. and St George-Hyslop P. H. (2002) gamma-Secretase, Notch, Abeta and Alzheimer's disease: where do the presenilins fit in? *Nat. Rev. Neurosci.* 3: 281-290.

Smith B. C., Fundamentals of Fourier Transform Infrared Spectroscopy, Second Edition ed., 2011.

Soares P. I., Alves A. M., Pereira L. C., Coutinho J. T., Ferreira I. M., Novo C. M. and Borges J. P. (2014) Effects of surfactants on the magnetic properties of iron oxide colloids. *J. Colloid Interface Sci.* 419: 46-51.

Soares P. I., Lochte F., Echeverria C., Pereira L. C., Coutinho J. T., Ferreira I. M., Novo C. M. and Borges J. P. (2015) Thermal and magnetic properties of iron oxide colloids: influence of surfactants. *Nanotechnology* 26: 425704.

Stuart B., Infrared Spectroscopy: Fundamentals and Applications, 2004.

Sun S. and Zeng H. (2002) Size-controlled synthesis of magnetite nanoparticles. *J. Am. Chem. Soc.* 124: 8204-8205.

Swanson H. E., Standard x-ray diffraction powder patterns, U.S. Dept. of Commerce For sale by the Supt. of Docs., U.S. G.P.O., Washington, DC, 1972.

Talelli M., Rijcken C. J., Lammers T., Seevinck P. R., Storm G., van Nostrum C. F. and Hennink W. E. (2009) Superparamagnetic iron oxide nanoparticles encapsulated in biodegradable thermosensitive polymeric micelles: toward a targeted nanomedicine suitable for image-guided drug delivery. *Langmuir* 25: 2060-2067.

Tartaj P., Morales M. P., Gonzalez-Carreno T., Veintemillas-Verdaguer S. and Serna C. J. (2011) The iron oxides strike back: from biomedical applications to energy storage devices and photoelectrochemical water splitting. *Adv Mater* 23: 5243-5249.

Teja A. S. and Koh P. Y. (2009) Synthesis, properties, and applications of magnetic iron oxide nanoparticles. *Progress in Crystal Growth and Characterization of Materials* 55: 22-45.

Trabulo S., Cardoso A. L., Mano M. and De Lima M. C. (2010) Cell-Penetrating Peptides-Mechanisms of Cellular Uptake and Generation of Delivery Systems. *Pharmaceuticals (Basel)* 3: 961-993.

Tycko R. (2016) Alzheimer's disease: Structure of aggregates revealed. *Nature* 537: 492-493.

Valenzuela R., Fuentes M. C., Parra C., Baeza J., Duran N., Sharma S. K., Knobel M. and Freer J. (2009) Influence of stirring velocity on the synthesis of magnetite nanoparticles (Fe3O4) by the co-precipitation method. *Journal of Alloys and Compounds* 488: 227–231.

Wahajuddin and Arora S. (2012) Superparamagnetic iron oxide nanoparticles: magnetic nanoplatforms as drug carriers. *Int J Nanomedicine* 7: 3445-3471.

Weiner M. W., Veitch D. P., Aisen P. S., Beckett L. A., Cairns N. J., Green R. C., Harvey D., Jack C. R., Jagust W., Liu E., Morris J. C., Petersen R. C., Saykin A. J., Schmidt M. E., Shaw L., Shen L., Siuciak J. A., Soares H., Toga A. W., Trojanowski J. Q. and Alzheimer's Disease Neuroimaging I. (2013) The Alzheimer's Disease Neuroimaging Initiative: a review of papers published since its inception. *Alzheimers Dement* 9: e111-194.

Wilhelm I. and Krizbai I. A. (2014) In vitro models of the blood-brain barrier for the study of drug delivery to the brain. *Mol. Pharm.* 11: 1949-1963.

Wisniewski T. and Frangione B. (1996) Molecular biology of brain aging and neurodegenerative disorders. *Acta Neurobiol. Exp. (Wars.)* 56: 267-279.

Wolburg H. and Lippoldt A. (2002) Tight junctions of the blood-brain barrier: development, composition and regulation. *Vascul. Pharmacol.* 38: 323-337.

Wu Y., Yang X., Yi X., Liu Y., Chen Y., Liu G. and Li R. W. (2015) Magnetic Nanoparticle for Biomedicine Applications. *Nanotechnology: Nanomedicine & Nanobiotechnology* 2.

Wyss-Coray T. and Rogers J. (2012) Inflammation in Alzheimer disease-a brief review of the basic science and clinical literature. *Cold Spring Harb. Perspect. Med.* 2: a006346.

Xie H., Zhu Y., Jiang W., Zhou Q., Yang H., Gu N., Zhang Y., Xu H., Xu H. and Yang X. (2011) Lactoferrin-conjugated superparamagnetic iron oxide nanoparticles as a specific MRI contrast agent for detection of brain glioma in vivo. *Biomaterials* 32: 495-502.

Yang L., Rieves D. and Ganley C. (2012) Brain amyloid imaging--FDA approval of florbetapir F18 injection. *N. Engl. J. Med.* 367: 885-887.

Zhang S., Chen X., Gu C., Zhang Y., Xu J., Bian Z., Yang D. and Gu N. (2009) The Effect of Iron Oxide Magnetic Nanoparticles on Smooth Muscle Cells. *NANO EXPRESS* 4: 70-77.

Zhang Y., Dringen R., Petters C., Rastedt W., Köser J., Filserd J. and Stolte S. (2016) Toxicity of dimercaptosuccinate-coated and unfunctionalized magnetic iron oxide nanoparticles towards aquatic organisms. *The Royal Society of Chemistry* 3: 754-767.

Zhang Y. W., Thompson R., Zhang H. and Xu H. (2011) APP processing in Alzheimer's disease. *Mol Brain* 4: 3.

Zheng H. and Koo E. H. (2011) Biology and pathophysiology of the amyloid precursor protein. *Mol. Neurodegener.* 6: 27.

Zou L. L., Ma J. L., Wang T., Yang T. B. and Liu C. B. (2013) Cell-penetrating Peptide-mediated therapeutic molecule delivery into the central nervous system. *Curr. Neuropharmacol.* 11: 197-208.

Appendix

Appendix I – Standard curve of Iron

Table A.1. Concentrations of iron (µg/ml) and respective absorbances.

Mohr's Salt (µg/ml)	Fe (µg/ml)	Abs (510 nm)		
		a	b	c
5	0,712	0,036	0,036	0,051
10,0	1,424	0,064	0,043	0,049
20,0	2,848	0,043	0,103	0,052
50,0	7,120	0,086	0,068	0,1017
75,0	10,681	0,094	0,122	0,086
100,0	14,241	0,143	0,121	0,125
250,0	35,602	0,215	0,22	0,199
500,0	71,204	0,295	0,264	0,286
750,0	106,805	0,435	0,474	0,413
1000	142,407	0,565	0,535	0,582
1250,0	178,009	0,624	0,697	0,628
1500,0	213,611	0,849	0,807	0,864

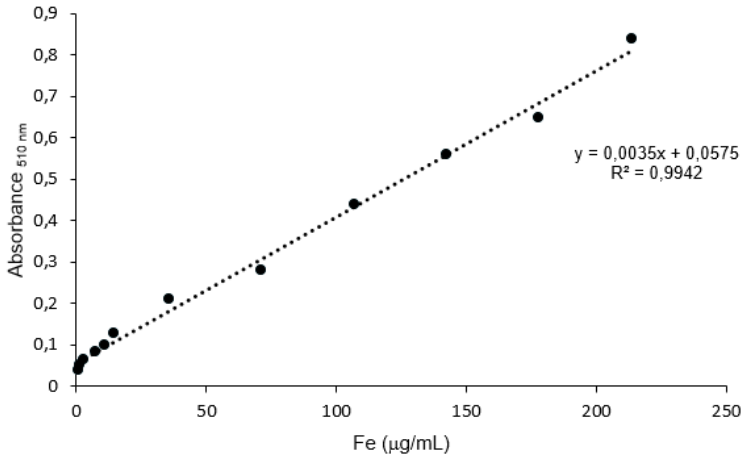

Figure A.1. Calibration curve of iron salt.

Appendix II – XRD Report by Match software

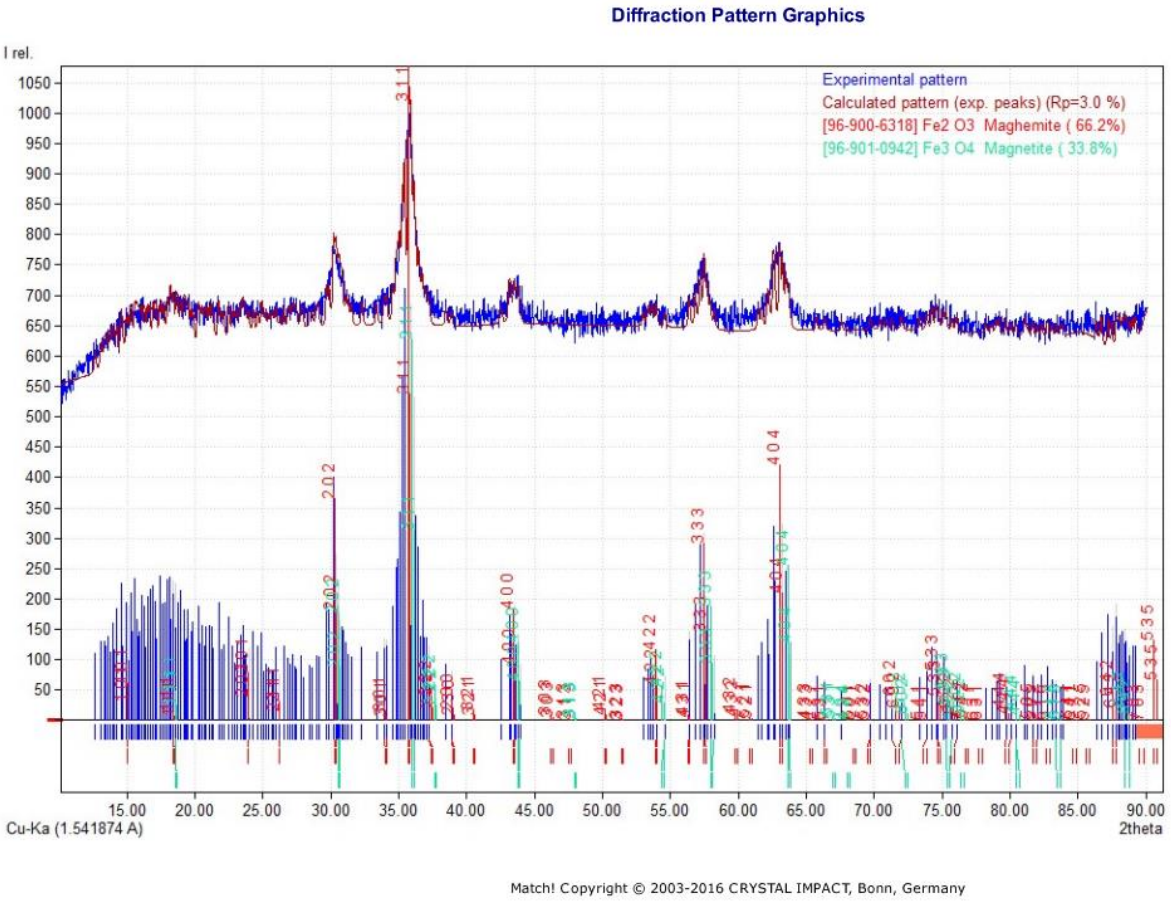

Figure A.2. Iron oxide species report obtained from the condition I by Match software.

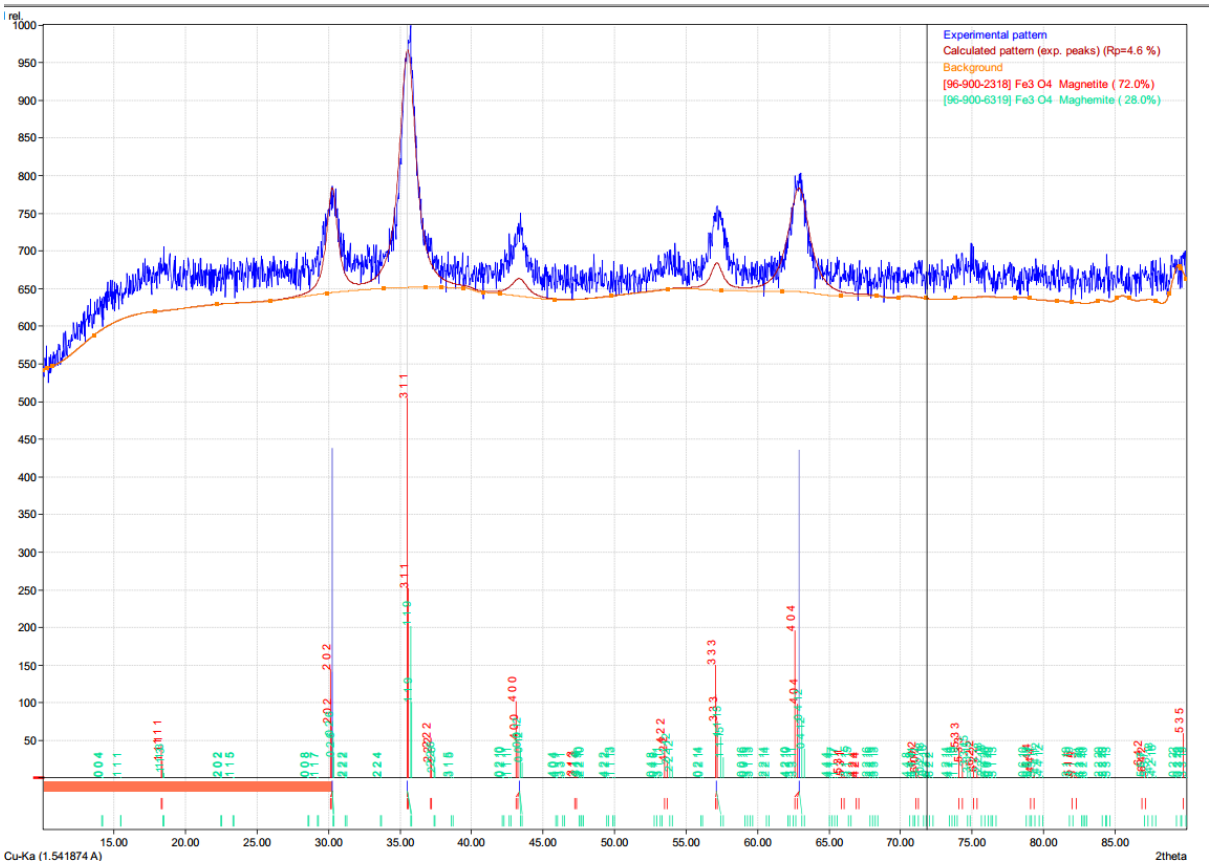

Figure A.3. Iron oxide species report obtained from the condition II by Match software

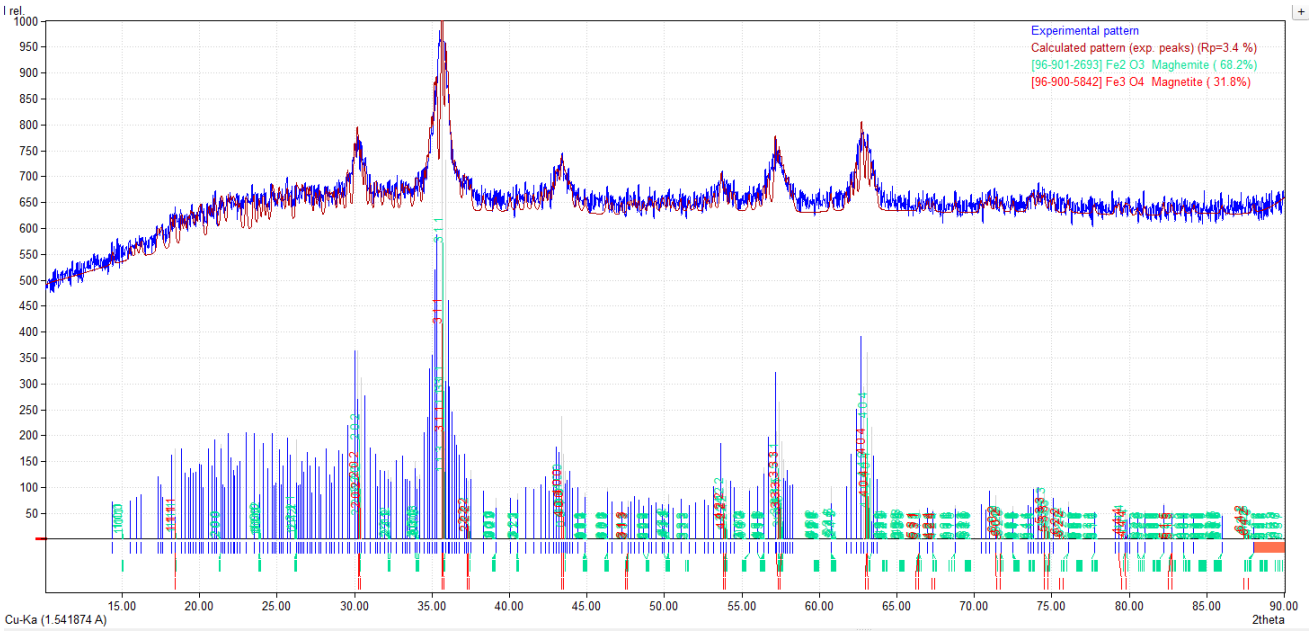

Figure A.4. Coated SPIONs with 0.3M DMSA report obtained by Match software.

Appendix III – Uptake assay of SPIONs-GFP-pepA

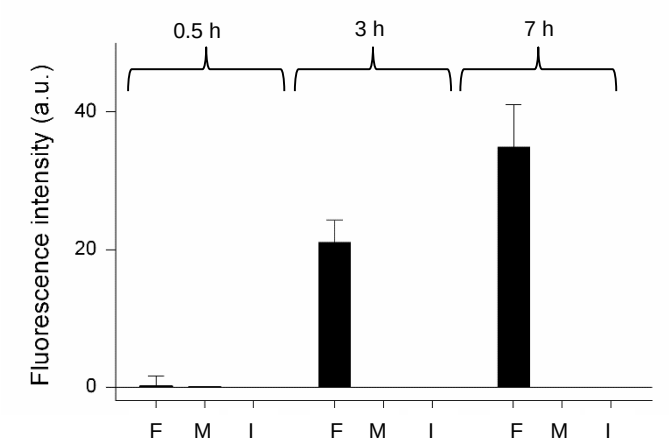

Figure A.5. Interaction with the cells membrane. 10 μg/ml SPIONs-GFP-pepA were incubated with bEnd.3 cells during 0.5, 3 and 7 h at 37 ºC, 5% CO_2. The fluorescence intensity of free media (F), membrane (M) and SPIONs-GFP-pepA internalized was measured at 395 and 509 nm, considering the GFP excitation and emission wavelength, respectively. The protein amount in the free media corresponds to the protein remaining in the upper chamber, the membrane protein amount corresponds to the protein released from the membrane with acid buffer and the internalized protein corresponds to the protein in the cell lysate. Values are mean ± SD, n = 3.